university of groningen

University Medical Center Groningen

University of Groningen

Mediterranean water in the Atlantic Iberian margin reveals early isolation events during the Messinian Salinity Crisis

Bulian, Francesca; Jiménez-Espejo, Francisco J.; Andersen, Nils; Larrasoaña, Juan C.; Sierro, Francisco J.

Published in:
Global and Planetary Change

DOI:
10.1016/j.gloplacha.2023.104297

IMPORTANT NOTE: You are advised to consult the publisher's version (publisher's PDF) if you wish to cite from it. Please check the document version below.

Document Version
Publisher's PDF, also known as Version of record

Publication date:
2023

Link to publication in University of Groningen/UMCG research database

Citation for published version (APA):
Bulian, F., Jiménez-Espejo, F. J., Andersen, N., Larrasoaña, J. C., & Sierro, F. J. (2023). Mediterranean water in the Atlantic Iberian margin reveals early isolation events during the Messinian Salinity Crisis. *Global and Planetary Change*, *231*, Article 104297. https://doi.org/10.1016/j.gloplacha.2023.104297

Copyright
Other than for strictly personal use, it is not permitted to download or to forward/distribute the text or part of it without the consent of the author(s) and/or copyright holder(s), unless the work is under an open content license (like Creative Commons).

The publication may also be distributed here under the terms of Article 25fa of the Dutch Copyright Act, indicated by the “Taverne” license. More information can be found on the University of Groningen website: https://www.rug.nl/library/open-access/self-archiving-pure/taverne-amendment.

Take-down policy
If you believe that this document breaches copyright please contact us providing details, and we will remove access to the work immediately and investigate your claim.

Downloaded from the University of Groningen/UMCG research database (Pure): http://www.rug.nl/research/portal. For technical reasons the number of authors shown on this cover page is limited to 10 maximum.

Global and Planetary Change 231 (2023) 104297

Contents lists available at ScienceDirect

Global and Planetary Change

journal homepage: www.elsevier.com/locate/gloplacha

Mediterranean water in the Atlantic Iberian margin reveals early isolation events during the Messinian Salinity Crisis

Francesca Bulian [a,e,*], Francisco J. Jiménez-Espejo [b,c], Nils Andersen [d], Juan C. Larrasoaña [f,g,h], Francisco J. Sierro [a]

[a] Departamento de Geología, Univ. de Salamanca, Plaza de los Caídos s/n, 37008 Salamanca, Spain
[b] Instituto Andaluz de Ciencias de la Tierra (CSIC-UGR), Armilla, Spain
[c] Research Institute for Marine Resources Utilization (Biogeochemistry Program), JAMSTEC, Yokosuka, Japan
[d] Leibniz-Laboratory for Radiometric Dating and Isotope Research, Christian-Albrechts-Universität zu Kiel, Max-Eyth-Str.11-13, 24118 Kiel, Germany
[e] Groningen Institute of Archeology, University of Groningen, Poststraat 6, 9712 ER, Groningen, the Netherlands
[f] CN IGME, CSIC, Unidad de Zaragoza, Campus Aula Dei, Avenida Montañana 1005, 50559 Zaragoza, Spain
[g] Departamento de Ciencias, Universidad Pública de Navarra, Campus de Arrosadia, 31006 Pamplona, Spain
[h] Institute of Advanced Materials and Mathematics INAMAT^2, Universidad Pública de Navarra, Campus de Arrosadia, 31006 Pamplona, Spain

ARTICLE INFO

Editor: Dr. Fabienne Marret-Davies

Keywords:
Messinian Salinity Crisis
Stable isotopes
Iberian margin
Mediterranean-Atlantic gateways

ABSTRACT

Recent studies highlight the role of the Mediterranean Outflow Water (MOW), in the intensification of the Atlantic Meridional Overturning Circulation and as source of heat and salty water to high latitudes. During the Late Miocene the MOW suffered major changes and likely a total collapse during the Messinian Salinity Crisis (MSC). In order to study the MOW evolution in the Atlantic margin during the Tortonian-Messinian interval we completed a new high resolution geochemical and stable isotope record for the corresponding interval of the Montemayor-1 and Huelva-1 cores. Both sites are located in the Guadalquivir Basin on the former Atlantic side of the Mediterranean – Atlantic gateways (Iberian Atlantic margin) during the late Miocene. The tuning of this isotope record with astronomical solutions and other global isotope curves has allowed the establishment of an improved chronology and, consequently, to precisely date environmental changes happening on the Atlantic margin of the Iberian peninsula and their link to Mediterranean and global events. At 7.17 Ma, in concomitance with a shallowing of the basin, the residence time, temperature and salinity of the bottom waters increased. These changes were related to a reduction of the MOW reaching the Atlantic side as a consequence of the restriction of the last strand of the Betic corridor that connected the Mediterranean and the Atlantic. This hypothesis is in line with the analogous changes observed in several Mediterranean Sea locations, where from 7.17 Ma onward a reduced Mediterranean – Atlantic connection is observable. Furthermore, the new isotope chronology sheds light, through comparison with other records, on the age of Messinian geomagnetic reversals.

1. Introduction

During critical periods of the Pliocene (Kaboth-Bahr et al., 2021) and the Pleistocene (Sierro et al., 2020) when the MOW played a major role in the Atlantic Meridional Overturning Circulation and northern high latitude ice formation, occasionally delaying the intensification of Northern Hemisphere glaciations (e.g., Kaboth et al., 2017). This is associated with the MOW as a relevant heat and salt source into the North Atlantic (Voelker et al., 2006) and as a teleconnection between low and high latitude climate cycles (Bahr et al., 2015; Rodrigo-Gámiz et al., 2014). Nevertheless, the role that the MOW could play during the major changes associated with the Late Miocene, e.g., intense reorganization of atmospheric circulation (Carrapa et al., 2019) affecting monsoon activity and westerlies (Christensen et al., 2021; Jöhnck et al., 2020) is less studied.

Today, the MOW formed in the Mediterranean Sea reaches the Atlantic Ocean through the Gibraltar Strait. This configuration has been present at least since the beginning of the Pliocene (e.g., Blanc, 2002; Garcia-Castellanos et al., 2009; Hsü et al., 1973; Roveri et al., 2014), when the Camarinal sill was breached and an efficient Mediterranean –

* Corresponding author at: Departamento de Geología, Univ. de Salamanca, Plaza de los Caídos s/n, 37008 Salamanca, Spain.
E-mail addresses: fra.bulian@usal.es (F. Bulian), francisco.jimenez@csic.es (F.J. Jiménez-Espejo), nandersen@leibniz.uni-kiel.de (N. Andersen), jc.larra@igme.es (J.C. Larrasoaña), sierro@usal.es (F.J. Sierro).

https://doi.org/10.1016/j.gloplacha.2023.104297
Received 26 June 2023; Received in revised form 18 October 2023; Accepted 2 November 2023
Available online 5 November 2023
0921-8181/© 2023 The Authors. Published by Elsevier B.V. This is an open access article under the CC BY-NC license (http://creativecommons.org/licenses/by-nc/4.0/).

Atlantic connection was established ending the dramatic event known as the Messinian Salinity Crisis (MSC; Hsü et al., 1973; Krijgsman et al., 1999b; Selli, 1973). During the 600 kyr that this event lasted (5.967–5.332 Ma; Manzi et al., 2013), a reduced or completely absent connection between the Atlantic Ocean and Mediterranean Sea led to the deposition of more than a kilometre thick succession of evaporites (e.g., CIESM, 2008 and references therein).

The progressive closure of the Mediterranean – Atlantic gateway that led to the MSC started already in the Tortonian, with the restriction of the Betic and Rifian corridors (Fig. 1) that acted as marine gateways since the Miocene (e.g., Bialik et al., 2019; Popov et al., 2004). Some studies have shown how the southern strand (the Rifian corridor) most probably closed between 7.1 and 6.9 Ma, while the northern (Betic) corridor closed around 7.35–7.25 Ma (Capella et al., 2018; Krijgsman and Langereis, 2000; Tulbure et al., 2017). In the Betic corridor, uplift started as early as ~7.8–7.6 Ma in the east and resulted in a progressive westward disconnection of the smaller basins (Guadix and Granada basins; Betzler et al., 2006; Corbí et al., 2012; Hüsing et al., 2010; Pineda et al., 2023). For the closure and infill of the Guadalhorce Corridor, different chronologies have been proposed ranging from Messinian (Martín et al., 2014; Pérez-Asensio et al., 2014) to Tortonian (Sanz de Galdeano and Alfaro, 2004; Van der Schee et al., 2018) in age. Having both the Betic and Rifian corridors closed before the onset of the MSC, the occurrence of another gateway seems mandatory in order to provide the necessary ions for the Mediterranean salt giant to precipitate. Recent studies suggest how a proto-Gibraltar strait might have been taking over the Mediterranean-Atlantic connectivity since the late Tortonian-early Messinian (Capella et al., 2020; Krijgsman et al., 2018).

More research is needed in order to better understand the chronologies of the opening and closure of the Gibraltar arch gateways, because the task has proven to be challenging. Due to the strong erosion that affected the Mediterranean basin at the onset of the MSC with the breach of the Gibraltar strait (Bulian et al., 2021; Garcia-Castellanos et al., 2019), identifying a complete Tortonian – Pliocene record to reconstruct the dynamics that led to the MSC has proven to be a difficult task. Additionally, even though there may have been marine sedimentation in the Betic straits during the Messinian (Capella et al., 2017; e.g., Corbí et al., 2012; Tulbure et al., 2017; Van der Schee et al., 2018), the deposits may have been eroded due to uplift (e.g., Fadil et al., 2006; Garcia-Castellanos and Villaseñor, 2011; Mancilla et al., 2015), making it very hard to find complete records of the gateway restriction (Flecker et al., 2015; Van der Schee et al., 2018). To solve the uncertainties related to the timing of the gateway closure, other studies have been carried out on the Atlantic margin using boreholes (i.e. Montemayor-1 and Huelva-1) drilled in the westernmost sector of the Guadalquivir Basin, where a continuous Tortonian-Pliocene record can be found and the influence of Mediterranean water masses studied (Fig. 1).

In particular, paleomagnetism (Larrasoaña et al., 2008; Larrasoaña et al., 2014), benthic foraminifer associations (Pérez-Asensio et al., 2013; Pérez-Asensio et al., 2014), content of major elements (Van den Berg et al., 2018; Van den Berg et al., 2015), stable isotope (Pérez-Asensio et al., 2012a, 2012b) and pollen records (Jiménez-Moreno et al., 2013) have been all acquired on the Montemayor-1 core. Using these data, an astronomical tuning was performed between 6.4 and 5.3 Ma. On the Huelva-1 core, stable isotope data are missing and only the paleomagnetism (Larrasoaña et al., 2008; Larrasoaña et al., 2014) and elemental composition based on X-ray Fluorescences (XRF) have been investigated (Van den Berg et al., 2018). Nonetheless, the astronomically tuned record of the core covers only the late Messinian (6.37–5.33 Ma), as does the geochemical dataset. This prevents us from investigating whether the first signs of restriction of the Gibraltar gateway(s), visible in the Mediterranean Basin since 7.17 Ma (Bulian et al., 2021; Kouwenhoven et al., 1999; Kouwenhoven, 2000; Kouwenhoven et al., 2003; Seidenkrantz et al., 2000), left their imprint on the Atlantic margin oceanography.

In this study, we set the focus on the late Tortonian-early Messinian interval in both the Montemayor-1 and Huelva-1 cores by significantly improving the astronomical tuning of the lower parts of both records, between 257.3 and 236 md (meters of depth) and 169.9–148.9 md, respectively. For the Montemayor-1 core, a new high-resolution geochemical dataset, including planktic and benthic stable isotopes and major element content, has been produced. In addition, we have generated a foraminifer stable isotope record for the late Tortonian–early Messinian in the Huelva-1 core because the lowermost part of Montemayor-1 was condensed. Having these two continuous datasets has enabled us to revise and refine the previous age models (Van den

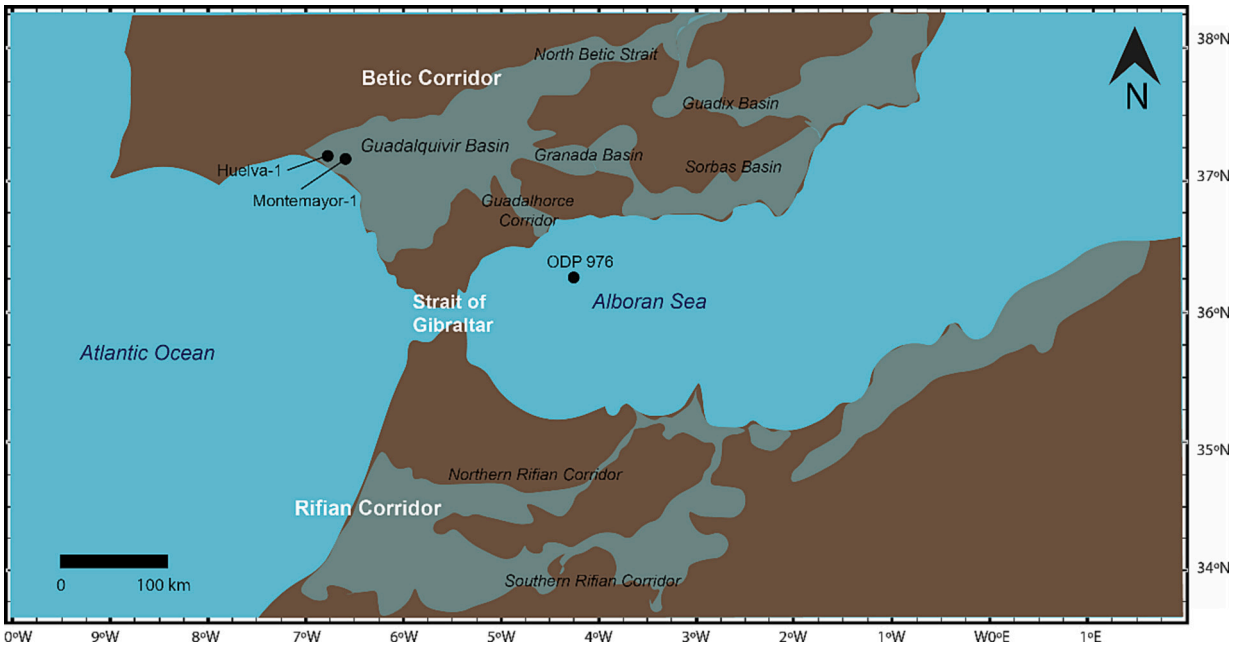

Fig. 1. Schematic map of the Alboran Sea area showing the location of the Montemayor-1 and Huelva-1 cores. The light-blue shading represents the area formerly occupied by the Betic and Rifian corridors (Capella et al., 2020). (For interpretation of the references to colour in this figure legend, the reader is referred to the web version of this article.)

Berg et al., 2018; Van den Berg et al., 2015) and to obtain a complete composite Tortonian-Messinian dataset for the Atlantic margin of the Gulf of Cadiz, encompassing the time interval during which the first Mediterranean gateway restriction took place. This composite dataset includes also a revision of the astronomical ages given to the magnetic chrons identified by Larrasoaña et al. (2008) and correlated to the Geomagnetic Polarity Time Scale GTS2012 (Hilgen et al., 2012) based on the cyclostratigraphic tuning of the Sorbas basin (Western Mediterranean; Krijgsman et al., 1999a; Sierro et al., 2001) with the ages provided by Drury et al. (2017) and accepted in the GTS2020 (Raffi et al., 2020), this way we have been able to investigate in detail the influence that MOW had on the Atlantic margin waters during the Mediterranean-Atlantic restriction.

1. Geological setting and core stratigraphy

The Guadalquivir Basin (GB) is a WSW-ENE elongated triangular basin located in the south of the Iberian Peninsula that formed during the late Serravallian-early Tortonian (Garcia-Castellanos et al., 2002; Sanz De Galdeano and Vera, 1992; Sierro et al., 1996). Towards the west it opens to the Atlantic Ocean, to the north it is limited by the Iberian Massif, and to the south it is bounded by the Betic Cordillera, constituting its foreland (González-Delgado et al., 2004; Sierro et al., 1996).

During the Early-Middle Miocene, the NW-directed convergence

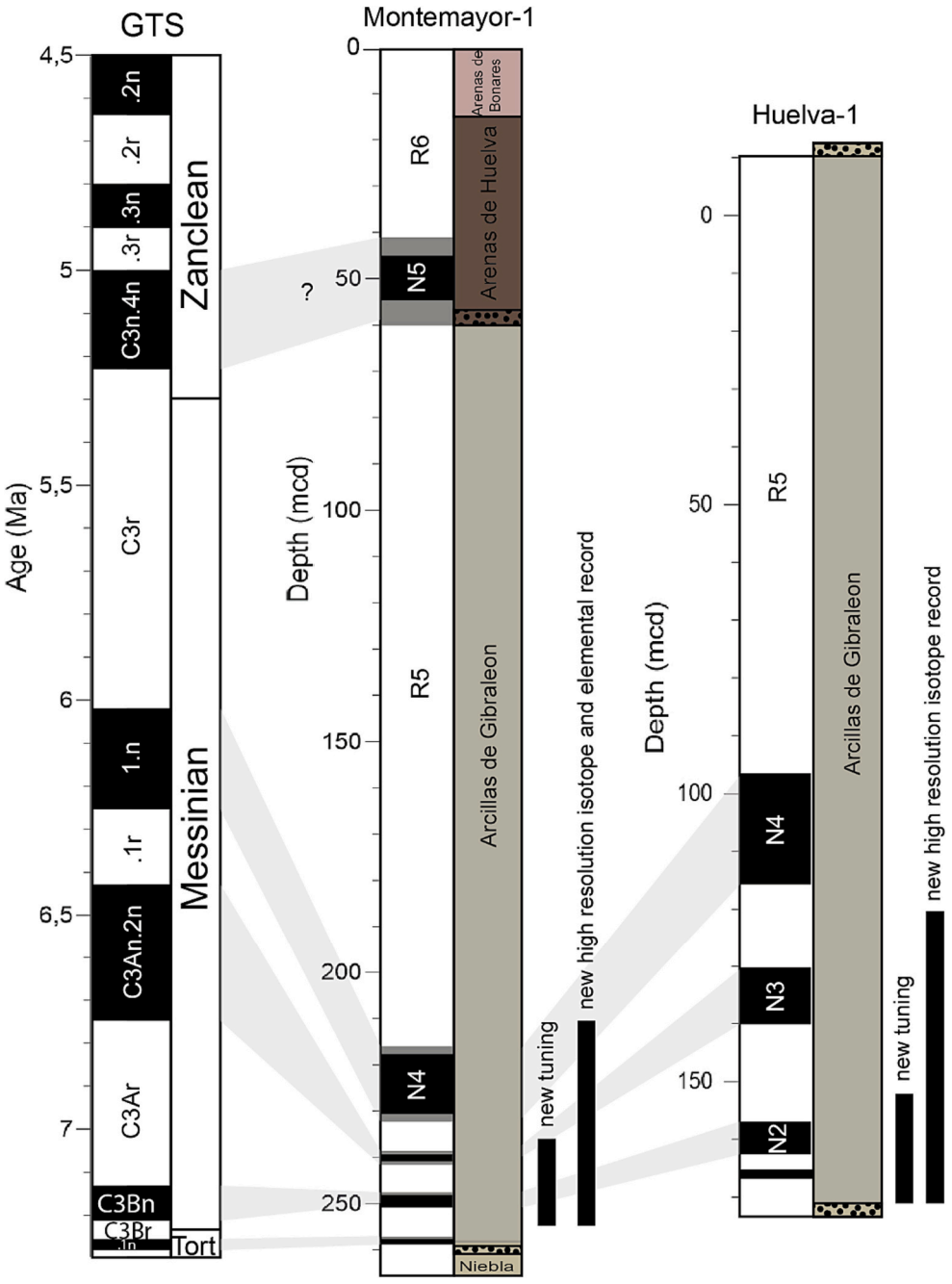

Fig. 2. On the left, the Tortonian – Zanclean magnetostratigraphic chrons from Lourens et al. (2004). In the Middle the magnetostratigraphic results for Montemayor-1 core (Larrasoaña et al., 2008; Larrasoaña et al., 2014) and the lithological column showing the different formations present in Montemayor-1 core (Niebla Formation, Arcillas de Gibraleón Formation, Arenas de Huelva Formation and Arenas de Bonares Formation). On the right, the magnetostratigraphic results for Huelva-1 core (Larrasoaña et al., 2008; Larrasoaña et al., 2014) and the lithological column showing the different formations present (Arcillas de Gibraleón Formation).

between the Eurasian and African plates caused the stacking of the Betic external tectonic units leading to the downward flexural subsidence of the Iberian basement and the subsequent infilling of the basin (Berástegui et al., 1998; Garcia-Castellanos et al., 2002; Ledesma, 2000; Sierro et al., 1996), which mainly witnessed continuous marine to continental sedimentation during the Tortonian – early Messinian. After the uplift of the Betic Cordillera, the GB became a large embayment and represented the Atlantic side of the Betic corridor, which, together with the Rifian passages in Morocco, enabled the connection between the Mediterranean Basin and the Atlantic Ocean (Benson et al., 1991; Martín et al., 2001). Here, warm and salty MOW leaving the Mediterranean encountered fresher and cooler Atlantic Upwelled Waters (AUW), forming a two-layered water column (Martín et al., 2001; Pérez-Asensio et al., 2012a, 2012b). The GB shows a continuous sedimentary fill composed of a lower marine sequence (late Tortonian – early Pliocene) and an upper continental sequence (Aguirre, 1992; González-Delgado et al., 2004; Salvany et al., 2011; Sierro et al., 1996). The lower part of the marine sequence shows huge sedimentary structures suggesting that Mediterranean waters were flowing out into the Atlantic at current velocities estimated at 1–1.5 m/s (Martín et al., 2001).

The Montemayor-1 (37°16′N, 6°49′W) and Huelva-1 (37°16′N, 6°57′W) cores were drilled in the north-western margin of the GB, a tectonically inactive area where the sedimentary sequence reaches its maximum thickness. The Montemayor-1 core (Fig. 2) is characterized at the base by 1.5 m of Paleozoic–Mesozoic substrate composed of reddish clays. The basement is overlain by the four lowermost lithostratigraphic units that characterize the GB sedimentary infill (González-Delgado et al., 2004; Sierro et al., 1996). The lowermost unit, 5 m thick, corresponds to the cemented carbonate-siliciclastic coastal deposits of the Niebla Formation (Tortonian), and are followed by 198 m of deep marine greenish-blue clays of the Arcillas de Gibraleón Formation (late Tortonian-Messinian). At the base of the of Arcillas de Gibraleón Fm, a 3 m-thick glauconitic layer can be identified. At 60 md (meters of depth) another glauconite layer separates the Arcillas de Gibraleón Fm from the 42 m-thick marine sands and silts of the Arenas de Huelva Formation (early Pliocene). This formation is capped by a discontinuity at 18 md, which is overlain by 14.5 m of brownish transitional sands of the Arenas de Bonares Formation (late Pliocene-Pleistocene) and 3.5 m of recent soil that mark the end of the core (Larrasoaña et al., 2008; Larrasoaña et al., 2014).

In the Huelva-1 core, the same basal units have been recognized (Fig. 2), including 4 m of the Niebla Fm and almost 176 m of the Arcillas de Gibraleón Fm. At 170 md and 12 md, two glauconitic layers at the base and top of the Arcillas de Gibraleón Fm have also been found (Larrasoaña et al., 2008; Van den Berg et al., 2018).

2. Materials and methods

2.1. Stable isotope analyses

In order to improve the resolution of the pre-existing stable isotope dataset (Pérez-Asensio et al., 2012a, 2012b; interval 240–210 md) and to complete the record until the base of the core (257.3 md), foraminifer shells from 405 samples of the Montemayor-1 core were analysed for stable isotopes ($\delta^{13}C$ and $\delta^{18}O$). Between 257 and 253.9 md numerous samples were barren and consequently, the continuous record starts at 253.9 md. Additionally, 402 samples from neighbouring the Huelva-1 core (170–120 md) were also analysed to improve the resolution of the lowest part of the Montemayor-1 record, which was condensed. When possible, a sampling step of 10 cm was applied to achieve high-resolution. The analyses were performed on ultrasonically cleaned 5–10 individuals of benthic foraminifer species *Cibicidoides pachyderma* and 10–20 specimens of planktic foraminifer *Globigerina bulloides*, picked from the >150 μm size fraction for each sample.

The analyses were performed with a Finnigan MAT 253 mass spectrometer connected to a Kiel IV carbonate preparation device at the Christian-Albrechts University in Kiel (Germany). Sample reaction was induced by individual acid addition (99% H_3PO_4 at 75 °C) under vacuum. The evolved carbon dioxide was analysed eight times for each individual sample. As documented by the performance of international [NBS19: +1.95 ‰ VPDB (^{13}C), −2.20 ‰ VPDB (^{18}O); IAEA-603: +2.46 ‰ VPDB (^{13}C), −2.37 ‰ VPDB (^{18}O)] and laboratory-internal carbonate standards [Hela1: +0.91 ‰ VPDB (^{13}C), +2.48 ‰ VPDB (^{18}O); HB1: -12.10 ‰ VPDB (^{13}C), −18.10 ‰ VPDB (^{18}O); SHK: +1.74 ‰ VPDB (^{13}C), −4.85 ‰ VPDB (^{18}O)], analytical precision of stable isotope analysis is better than ±0.08 ‰ for $\delta^{18}O$ and better than ±0.05 ‰ for $\delta^{13}C$. The obtained values were calibrated relative to Vienna Pee Dee Belemnite (VPDB).

2.2. Major and minor element analysis

Because cyclical changes in the sediment chemical composition were recognized and used for astronomical tuning of the 237–60 md interval of the Montemayor-1 core (Van den Berg et al., 2018; Van den Berg et al., 2015), we performed XRF analyses on the 253.7–237 md interval to have a complete geochemical dataset and improve the tuning of the entire record. A total of 162 samples was taken every 10 cm; each one was grinded to fine powder in an agate mortar, subsequently obtaining tablets of 10 mm in diameter with a manual press with a load of 5 Tm. The tablets were fixed on a glass slide to facilitate their handling. On each tablet, which were prepared with sufficient thickness to avoid transparency phenomena, 25 random points were measured for 30 s with a Bruker M4 Tornado Spectrometer where the generator parameters were set at 50 kV and 150 μA. A representative spectra and semi-quantitative results of each sample were obtained using the ESPRIT software, set at international standards. This analysis was performed at the General Service of X-ray diffraction at University of Salamanca (Nucleus).

The results obtained for the major elements were expressed in wt% (weight %) of the oxide, while the minor elements were expressed in ppm (parts per million) of the element. To make the dataset comparable to the published geochemical record, the wt% of each oxide was transformed into the wt% of the element itself. To do so, every oxide wt% was multiplied by its atomic weight and then divided by the atomic weight of the major element (Ragland, 1989). Furthermore, the values of the light elements that were expressed in ppm were transformed in wt%.

2.2.1. Statistics

To investigate the different factors influencing the geochemical composition and to distinguish between sedimentary processes, Principal Component Analysis (PCA) was used in conjunction with PAST 4.05.

Software© (Hammer et al., 2001) considering every element as a variable. PCA is a well-established dimension-reducing statistical technique, applied for pattern recognition in multivariate datasets (Abdi and Williams, 2010). The calculated eigenvalues give a measure of the variance accounted for by the corresponding components (axes of the PCA). As data pre-treatment, each value was converted to z-scores to eliminate the bias caused by the differences in the element concentrations following the next formula $Z(Xi) = (Xi - \check{u}\ (X1, X2, \ldots.Xz))/\sigma\ (X1, X2, \ldots.Xz)$, where X represents the selected ratio, ŭ and σ are the mean and the standard deviation of the dataset, respectively. Finally, to enable a direct appraisal between the new data presented here and the PCA previously obtained by Van den Berg et al. (2015), the same elements were included in the analyses (Fe, Al, Ca, Ti. Zr, Si, K, Rb and Sr).

2.3. Planktic foraminifer analyses

To identify the main bioevents, a quantitative study of the planktic foraminiferal content was performed on 236 samples from the Montemayor-1 core covering the 257–198.5 md interval. The core was sampled with an increasing upward resolution, ranging from 0.2 m at

the base to 1 m at the top of the studied interval to account for the reported increase in sedimentation rate (Van den Berg et al., 2018; Van den Berg et al., 2015). Each sample was dried in the oven, disaggregated in water overnight and subsequently washed over a > 150 μm and > 63 μm sieve. From the >150 μm fraction at least 300 planktic foraminifer specimens were classified into species and counted under a microscope. For both cores, the sum of the >63 μm and > 150 μm grain % fraction was calculated and considered to represent the sand content.

2.4. Spectral analyses

To establish the nature and significance of the periodic changes in the stable isotope dataset of Montemayor-1, a spectral analysis was performed. The analysis was carried out using Past software (Hammer et al., 2001) with the Redfit procedure, which allows to assess datasets with uneven sampling steps. The spectral peaks higher than the 95% confidence interval were considered significant as based on Monte Carlo methods.

3. Results

3.1. Stable isotope record

The stable isotope data from 257 to 209 md of Montemayor is shown in Fig. 2. The planktic $\delta^{18}O$ curve shows a stable trend with values around 0.2 and − 0.2 ‰ until 234 md of depth, when they drop to minimum values of ~ − 0.4 ‰. At the depth of 225 md, the planktic $\delta^{18}O$ curve rises again towards higher values, stays around ~0.2 ‰ for the next 10 m, and decreases again till reaching a minimum of ~ − 0.6 ‰. The general trend of the benthic $\delta^{18}O$ curve displays a similar pattern as the planktic record, with analogous minima and maxima. Nonetheless, a change towards higher values is visible at 245 md, where there is an increase from ~0.6 ‰ to ~0.8 ‰ that persists until the end of the record. In both the planktic and benthic $\delta^{13}C$ curves, there is a visible decreasing upwards trend. In the planktic record the latter is more gradual, so that it shifts from ~0.5 ‰ at the bottom to ~ −1 ‰ at the top of the section. The benthic record shows a more abrupt shift that can be pinpointed at 248 md, where a drop from ~1.5 ‰ to ~0.5 ‰ is recorded. This later value persists until 216 md, when the curve almost reaches 0 ‰.

The sand content (Fig. 3) in Montemayor is high, reaching up to 80% in the first 6 m of the core. From 254 md onward, the sand content decreases and stays around 10–15% throughout the rest of the analysed section.

The stable isotope data of the 170–120 md interval of the Huelva-1 core is shown in Fig. 4. The planktic $\delta^{18}O$ curve shows a stable trend with values around 0.6 and − 0.4 ‰, with stronger negative oscillations at 154 and 149 md (where values of −1 and − 0.8 ‰ are reached, respectively). The benthic $\delta^{18}O$ curve shows an analogous trend like the planktic record and fluctuates on average between 1 ‰ and 0.3 ‰, with the highest amplitudes found between 160 and 149 md, where values between 1.2 and 0.1 ‰ are reached. In both the planktic and benthic $\delta^{13}C$ curves there is a decreasing upward trend. In the planktic record such trend is more subtle, so that values of ~0.25 ‰ are registered at the bottom whereas values down to ~ −0.75 ‰ are found at the top of the section. As it happened in the Montemayor-1 record, the benthic $\delta^{13}C$ curve shows a more abrupt shift, especially after 160 md, where the curve shifts from ~1.5 ‰ to ~ − 0.5 ‰.

The sand content in Huelva (Fig. 4) is generally low, with only 7 peaks reaching values between 20 and 55%.

3.2. Statistical analysis

To make the data matrix visualization easier and to highlight the relationship between the elements, a PCA analysis was performed on the newly acquired geochemical data of Montemayor-1. The first two statistically significant principal components account for 81% of the total variance, with PC1 and PC2 describing its 66.1% and 15.06%, respectively.

The two most important negative loadings for PC1 are Ca and Sr (elements associated with carbonate content; Fig. 5 a), while the positive loading comprises the rest of the elements, including Al, Si, K, Ti, Fe, Rb and Zr (detrital input). In our site PC1 is interpreted as the dilution effect between terrigenous and carbonate fraction.

For PC2 (Fig. 5 b), the negative loading is represented mostly by Zr (typically associated with heavy minerals and coarse fractions), and to a lesser extent by Si and Fe, while on the positive side Al, Sr and Rb are

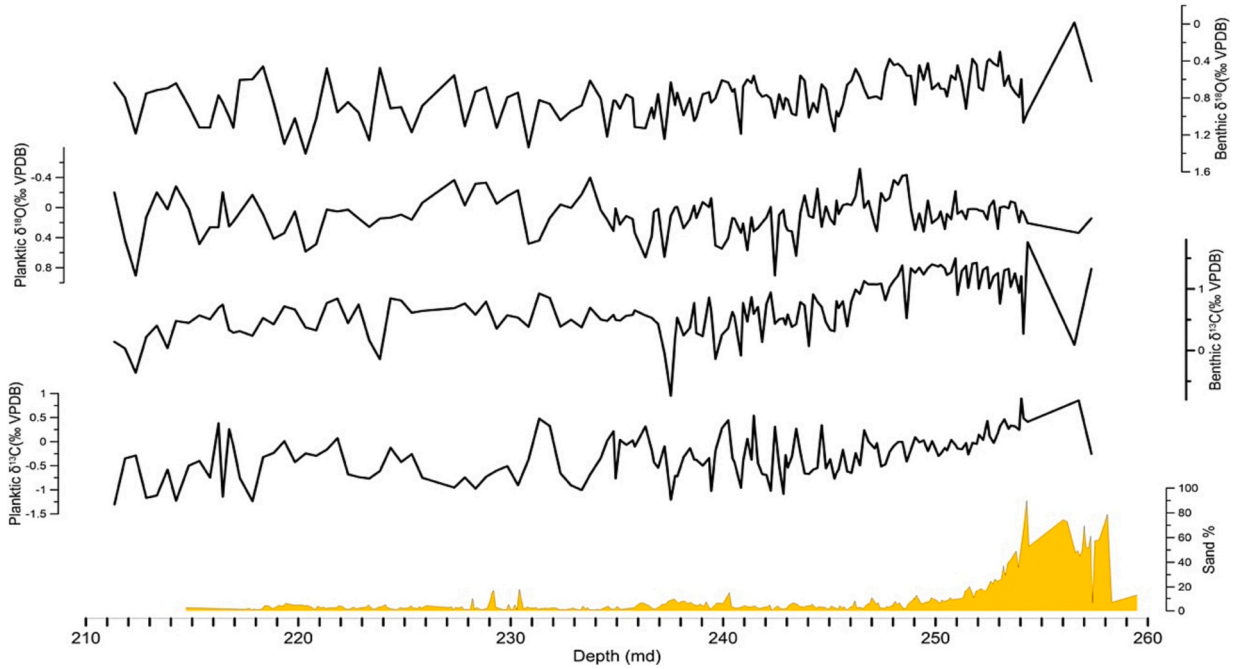

Fig. 3. Graph showing the abundance of sand fraction (%), the $\delta^{13}C$ and the $\delta^{18}O$ stable isotope data measured from benthic and planktic foraminifer shells record (*C. pachyderma* and *G. bulloides*) of Montemayor.

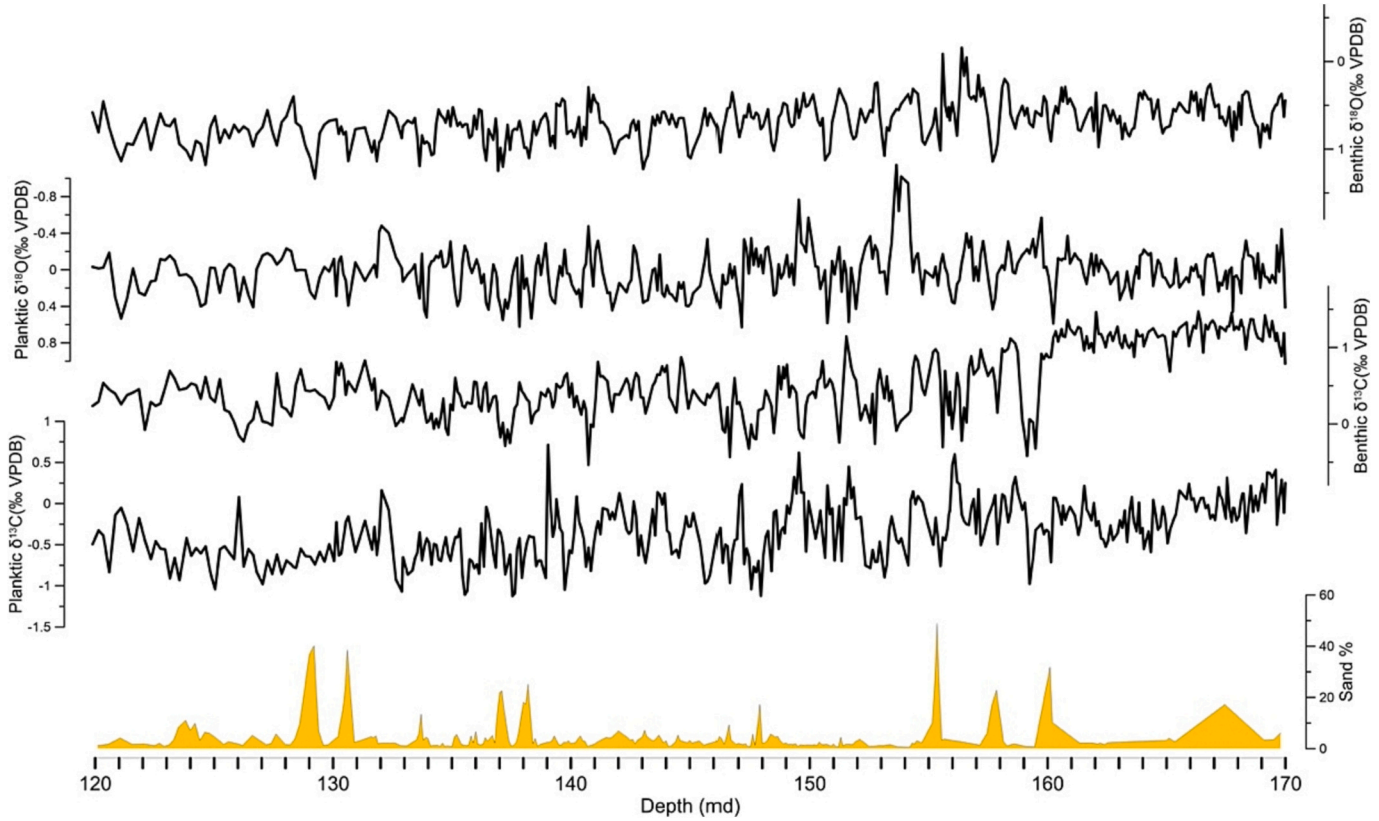

Fig. 4. Graph showing the abundance of sand fraction (%), the $\delta^{13}C$ and the $\delta^{18}O$ stable isotope data measured from benthic and planktic foraminifer shells record (*C. pachyderma* and *G. bulloides*) of Huelva.

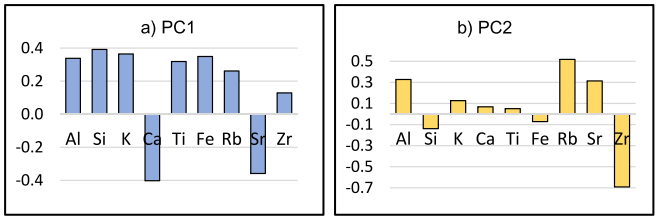

Fig. 5. Loadings of the Principal component performed on the geochemical record of Montemayor: a) PC1 and b) PC2.

dominant (Al and Rb associated with clay content and fine-grained particles).

The PC1 scores record (Fig. 6) shows positive values (less carbonates) from 253 md to the bottom, with an undulating pattern along the record. On the contrary, the PC2 record (Fig. 6) shows negative values (high Zr, Si and Fe) in the core bottom, associated with the sandy layers (Fig. 2), and quite stable values along the rest of the core, except punctual outliers.

4. Age model

4.1. Initial tie points

To build a first age model for the lower part of Montemayor (257.3–236 md) and Huelva (170–119.85 md) cores, several tie points were used based on the astronomical ages of planktic foraminifer bio-events (Fig. 7; Table 1) from this work and already published in Van den Berg et al. (2018). The planktic foraminifer biostratigraphic framework used is based on recent astronomically calibrated charts compiled by Lirer et al. (2019), while the numbering of each bioevent is taken from Sierro et al. (1993); Table 1).

In Montemayor-1 core, the Last Common Occurrence (LCO) of

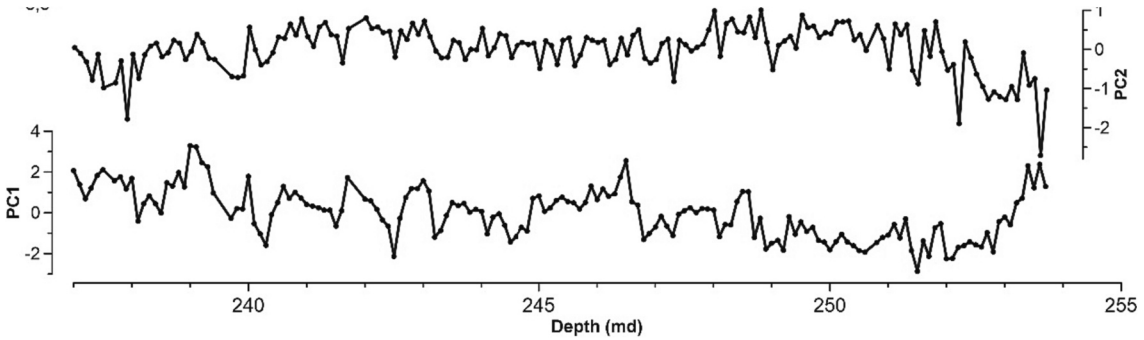

Fig. 6. Montemayor geochemical records in depth domain: a) PC1 scores; b) PC2 scores.

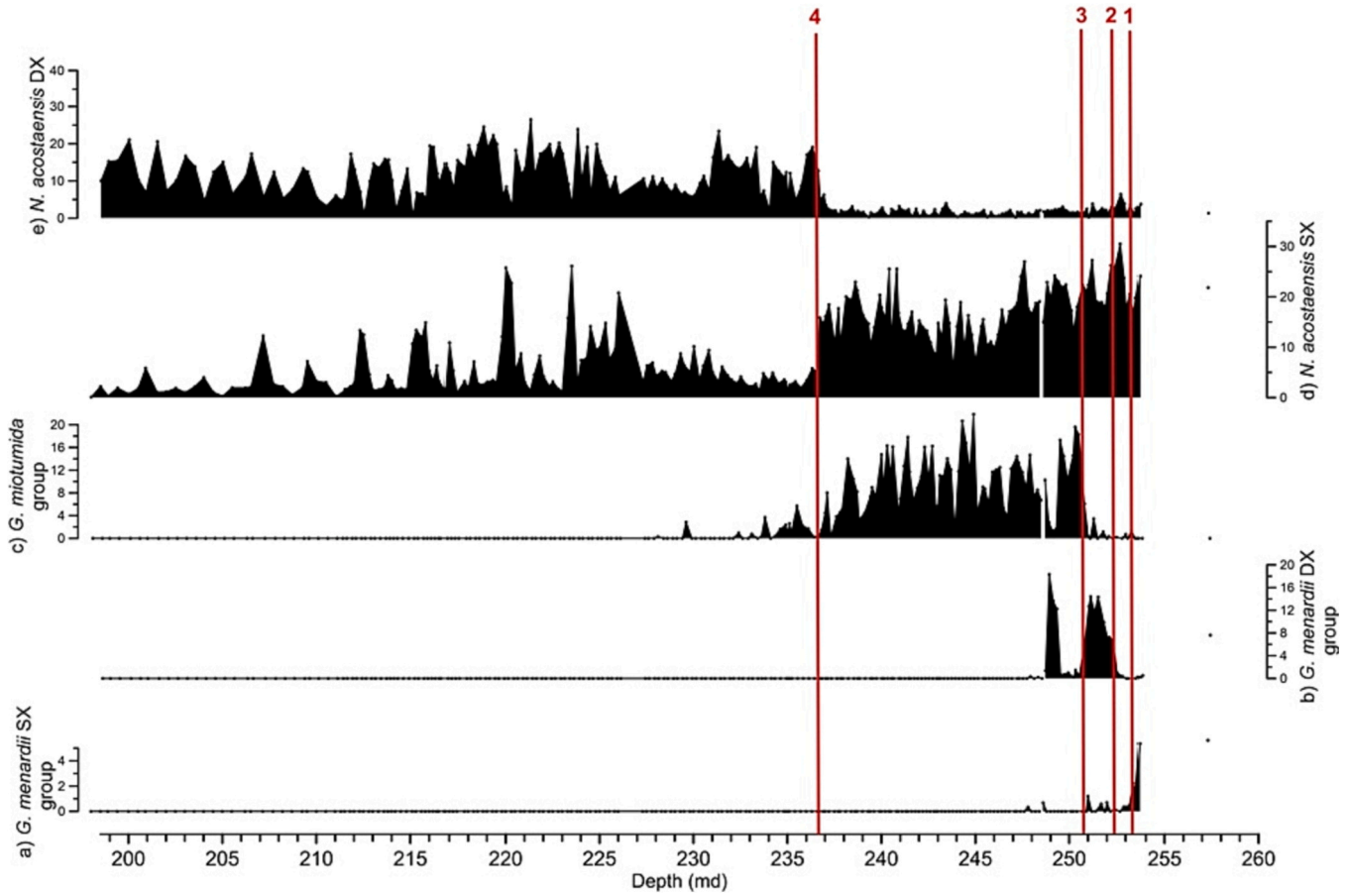

Fig. 7. The distribution of the main planktic foraminifer biostratigraphic markers found in Montemayor. The vertical lines and numbers denote the events of (Sierro et al., 1993).

Table 1
Planktic foraminifer bioevents used as initial tie points for the tuning of Montemayor and Huelva. The biostratigraphic scheme relies on Lirer et al. (2019) while the numbering of the bioevents is taken from Sierro et al. (1993).

Event	Astronomically calibrated age (Ma)	Depth (md) Montemayor-1 (this work)	Depth (md) Huelva-1 (Van den Berg et al., 2018)	N°
S/D coiling *N. acostaensis*	6.35 Ma	236.5 m	124.6 m	4
FCO *G. miotumida* group	7.24 Ma	250.4 m	165.25 m	3
FCO *G. menardii* 5 group (dextral)	7.36 Ma	252.4 m	168.35 m	2
LCO *G. menardii* 4 group (sinistral)	7.51 Ma	252.9 m	/	1

G. menardii 4 group has been located at 252.9 md. This event has been recognized in the NE Atlantic and the Mediterranean by Sierro (1985) and Sierro et al. (1993), and it has been astronomically calibrated at 7.51 Ma (Hilgen et al., 2000a; Hilgen et al., 2000b; Lourens et al., 2004). The next bioevent found is the First Common Occurrence (FCO) of *G. menardii* 5 group (Sierro, 1985; Sierro et al., 1993), recognized at 252.4 md and dated at 7.36 Ma (Hilgen et al., 2000a; Hilgen et al., 2000b; Lourens et al., 2004). In the NE Atlantic, the Tortonian – Messinian boundary (7.24 Ma; Hilgen et al., 2000a; Hilgen et al., 2000b; Lourens et al., 2004) is characterized by the replacement of the *G. menardii* 5 group by the *G. miotumida* group (Sierro, 1985; Sierro et al., 1993; Tjalsma, 1971). In Montemayor, this replacement happens at 250.4 md; however, at 250 md, *G. menardii* 5 group reappears again with high values and lasts for one more meter until 249 md (Fig. 7). Finally, at 236.5 md, the *N. acostaensis* coiling change from sinistral to dextral can be clearly identified (Fig. 7). The latter has been recognized from NE Atlantic cores (Sierro, 1985; Sierro et al., 1993) and Mediterranean outcrops (Hüsing et al., 2009; Sierro et al., 2001), where it has been astronomically tuned at 6.35 Ma (Hilgen and Krijgsman, 1999; (Lourens et al., 2004; Sierro et al., 1993; Sierro et al., 2001). All the pointers used for the tuning of the lower part of Montemayor core (257.3–236 md) are reported in Table 1.

For Huelva, events 2, 3 and 4 from Van den Berg et al. (2018) have been used (Table 1).

4.2. Astronomical tuning and composite section

Previous studies performed on the Montemayor and Huelva cores (Van den Berg et al., 2018; Van den Berg et al., 2015), as well as other boreholes in the GB like Casanieves (Ledesma, 2000), show how the late Messinian-early Pliocene sedimentation is mainly controlled by a climatic cyclicity related to astronomical forcing, whereby Northern Hemisphere summer insolation maxima and minima are marked by cyclical changes in the terrigenous and biogenic contents in the sediments.

The cyclicity in Huelva, as shown by Van den Berg et al. (2018), is clearly controlled by climate so that lower values of Ca-Sr/rest (see in Van den Berg et al., 2018; carbonates vs. terrigenous) have been tuned with maximum Northern Hemisphere summer insolation, and vice versa

(Fig. 7, black arrows). These records show very well the eccentricity-driven cycles as well, where minima in eccentricity corresponded with maxima in carbonate deposition (Fig. 7, black vertical lines). We know that, apart from the cyclicity related with changes in sediment input to the basin, warm-water foraminifers proliferate during insolation maxima at the same time that $\delta^{18}O$ values are lower in response to warmer and fresher surface waters, which concur with lower ice volumes (Rohling and Cooke, 1999). In addition, assuming that glacial cycles with higher benthic $\delta^{18}O$ occur at times of lower inclination of the Earth's axis, as it occurred during Pliocene-Pleistocene glacial cycles (Lisiecki and Raymo, 2005), it is possible to link benthic $\delta^{18}O$ maxima and obliquity minima. Consequently, the new $\delta^{18}O$ data provided in this study can be used to verify the existing astronomical tuning (Van den Berg et al., 2018), especially for the 7.1 to 7.4 Ma interval, where the element ratios do not show a very clear cyclicity (Fig. 8). Minor adjustments are needed in the lowermost part of the record to improve the astronomical tuning and to correlate the minima in obliquity and maxima in benthic $\delta^{18}O$, well visible from our data (Fig. 8, red vertical lines and red arrows). These modifications provide a more robust astronomical tuning of the lower part of the Huelva-1 core, where a clear cyclical pattern was identified in the $\delta^{18}O$ of both planktic and benthic records.

For Montemayor, an analogous cyclical pattern has been identified by Van den Berg et al. (2015) from 6.35 Ma until 5.85 Ma, where peaks in terrigenous material (high values of PC1) were tied to insolation maxima to create an age model (Fig. 9, black arrows). We applied the same tuning on the newly acquired benthic $\delta^{18}O$ record and found how each insolation maxima peak corresponded to an isotope minimum (Fig. 9). For the lowermost part of Monteamyor-1, no astronomical tuning was available considering that neither elemental nor stable isotope records were available. Our new data allowed to complete both records until the base of the core (Fig. 10). To do so, planktic foraminifer bioevents (Table 1, Fig. 7) were used as first-order tie points; for a more detailed astronomical tuning, the same relationships between cycles were assumed. Unfortunately, because the sedimentation rate is very low and the record very condensed, it was not possible to have a resolution at precessional scale. In contrast, eccentricity cycles are well visible and enable a lower resolution tuning; to facilitate such tuning between eccentricity maxima (in Fig. 10 each cycle is delimitated by black vertical lines), peaks in terrigenous input (high PC1), and minima in planktic and benthic $\delta^{18}O$, a spectral analysis was performed on the planktic $\delta^{18}O$ record, which shows the most pronounced cyclicity. It yielded cycles of 1.31 m, which were then tuned to the eccentricity record (Laskar et al., 2004), which modulates the amplitude of precession (Fig. 10).

After all these procedures, we have been able to produce a composite but continuous isotope record of the Iberian Atlantic Margin of the GB (Fig. 11) from the late Tortonian (7.4 Ma) to the base of the Pliocene (5.33 Ma). For the uppermost part of the record (5.76–5.33 Ma), we used the already published stable isotope curve of Montemayor from Pérez-Asensio et al. (2012a, 2012b). For the interval between 6.36 Ma and 5.76 Ma, the stable isotope record presented in this study for the Montemayor-1 core was also used because the cyclicity becomes more visible and marked by precession. On the other hand, for the lowermost interval (7.4–6.36 Ma), and because of the low sedimentation rates observed at the Montemayor-1 core during the late Tortonian–early Messinian, we used the Huelva-1 stable isotope record (Fig. 11), which shows a clearer precession cyclicity due to its higher sedimentation rates.

4.3. Astronomical ages of the magnetic polarity reversals during the Messinian

The new updated age model of the two sites has enabled the construction of a complete, high-resolution stable isotope record of the Guadalquivir basin from the base of the Pliocene to the late Tortonian. The modified tuning of the lower interval of Huelva (7.4 Ma to 7.1 Ma), and the new tuning of Montemayor (7.5 Ma to 6.4 Ma) has been made without using the magnetic chrons identified by Larrasoaña et al. (2008). There are some discrepancies in the dating of the Messinian

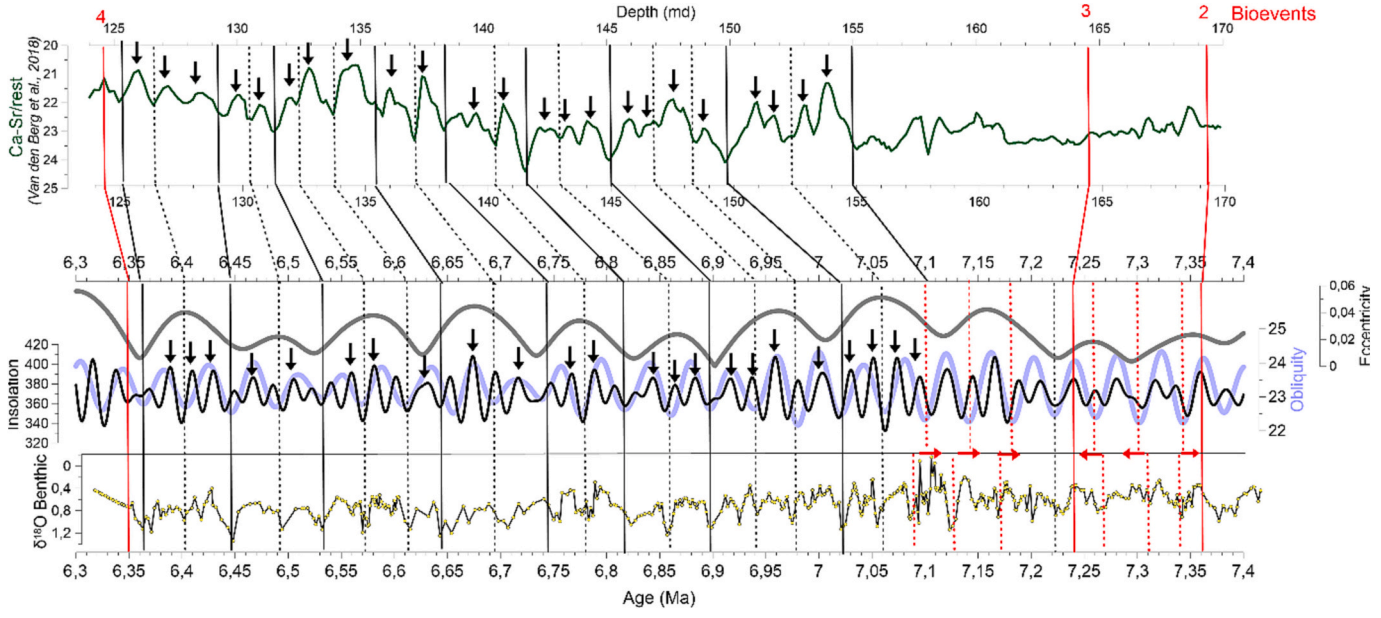

Fig. 8. Astronomical tuning of Huelva. Top: the Ca-Sr/rest ratio used for tuning by Van den Berg et al. (2018) where the black arrows indicate the most prominent insolation peaks used in the tuning. Bottom: astronomical target curves (eccentricity, obliquity and insolation) from Laskar et al. (2004) where the black arrows indicate the most prominent insolation cycles used for the astronomical tuning. Below, the benthic foraminifer $\delta^{18}O$ curve (this work) used for revising the existing tuning (Van den Berg et al., 2018). The red vertical lines show the main planktic foraminifer bioevents (Sierro et al., 1993; Lirer et al., 2019) used as initial tie points, the full black lines show the eccentricity minima, while the discontinuous black ones indicate the obliquity minima phases. The red dotted vertical lines paired with the red horizontal arrows highlight the improvements done to the age model based on the new stable isotope dataset. (For interpretation of the references to colour in this figure legend, the reader is referred to the web version of this article.)

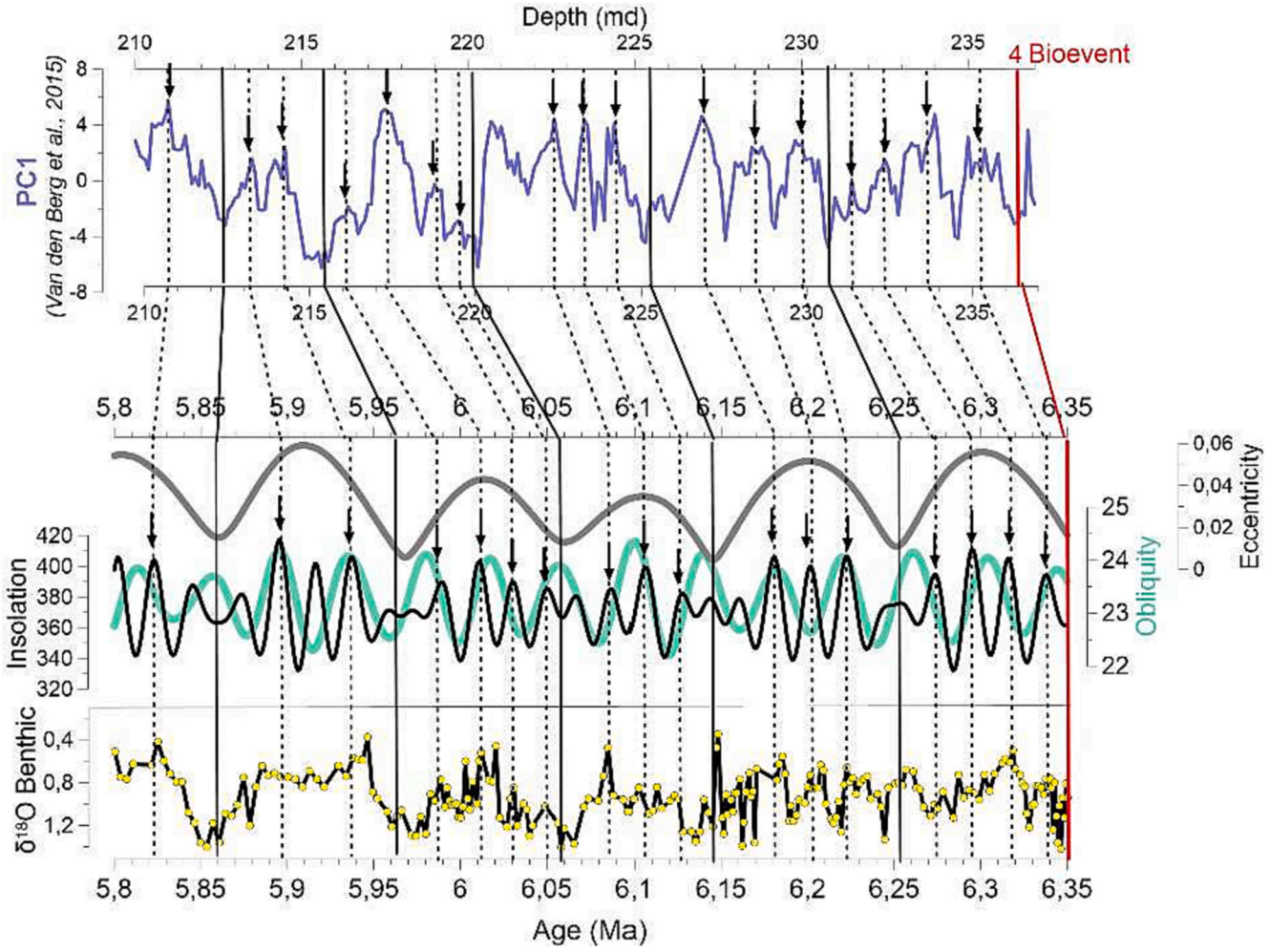

Fig. 9. Astronomical tuning of the upper part of the Montemayor record (6.35 to 5.8 Ma). On top, the PC1 curve (high values of PC1 indicate more detrital input) is shown (Van den Berg et al., 2015). In the bottom, the astronomical target curves (eccentricity, obliquity and insolation) are shown (Laskar et al., 2004) together with their correlation with the PC1 record where the tuned insolation peaks are highlighted by the black arrows and dashed lines. Below, the benthic $\delta^{18}O$ record of Montemayor (this study) is reported tuned with the pointers proposed from Van den Berg et al. (2015) where the most prominent insolation peaks are highlighted by the dotted vertical lines. In red, the planktic foraminifer bioevent is showed. (For interpretation of the references to colour in this figure legend, the reader is referred to the web version of this article.)

magnetic polarity reversals, in particular the ages of the top of the C3An.2n and C3Bn and the top and bottom of the C3An.2n magnetic chrons. The ages of these magnetic reversals in the GTS2004 and GTS2012 scales were based on the astronomical tuning of the Abad section in the Sorbas Basin (Krijgsman et al., 1999a; Sierro et al., 2001). However, more recently, Drury et al. (2017), based on high resolution data from DSDP Site U1337, where the magnetic signal is quite strong, has proposed new ages for the magnetic reversals comprised between 7.4 Ma and 6.3 Ma (chrons C3Br.1n, C3Bn and C3An.2n), which are slightly different from those reported in GTS2012 and have been accepted in the new GTS2020 (Raffi et al., 2020).

Based on the new tuning of the Montemayor and Huelva records, we have elaborated an astronomically tuned chronology for the magnetozones identified by Larrasoaña et al. (2008) that can be compared with those of the Abad and DSDP Site U1337 sections (Fig. 12, Table 2). Chron C3Br.1n was only identified in Huelva; sedimentation in Montemayor was condensed and precludes its identification. The next Chron, C3Bn, was identified in both records giving very consistent ages. The base of C3An.2n was evident in Huelva, while the top was more difficult to interpret. We challenge the original interpretation of Larrasoaña et al. (2008), and locate its top after a sequence of positive and negative inclination peaks, which were caused most probably by a delayed magnetization related with the presence of magnetofossils as already pointed out by Larrasoaña et al. (2014). Due to low sedimentation rates, this chron cannot be well defined in Montemayor.

Our new astronomical ages are in better agreement with those proposed by Drury et al. (2017) for the studied time interval (7.5 Ma – 6.3 Ma) with some small offsets. The new ages for the polarity magnetic reversals based on the astronomical tuning of Montemayor and Huelva are given in Table 2. The top and bottom of reversal C3Br.1n are concordant in the north Pacific, Sorbas Basin and Huelva, only the bottom of C3Br.1n is one precession cycle older in Sorbas Basin. Similar consistent ages are also given in the three records for the bottom of chron C3Bn, although its top, according to our data, is 20 and 40 kyr older than that recorded in the north Pacific and Sorbas, respectively (Table 2). For both the top and bottom of chron C3An.2n, we estimate an age 20 kyr older than Drury et al. (2017). The greatest change is registered for the top of C3An.2n since its age changes from 6.43 Ma in Sorbas Basin to 6.37 Ma based on our new tuning of the polarity magnetic reversals. This age is only 20 kyr younger than that registered by Drury et al., 2017 in the north Pacific.

Because of the new polarity ages in the Pacific, Drury et al. (2017) suggested that the Oued Akrech section (Hilgen et al., 2000a) could have a different age by a few precessional cycles as well as the Abad

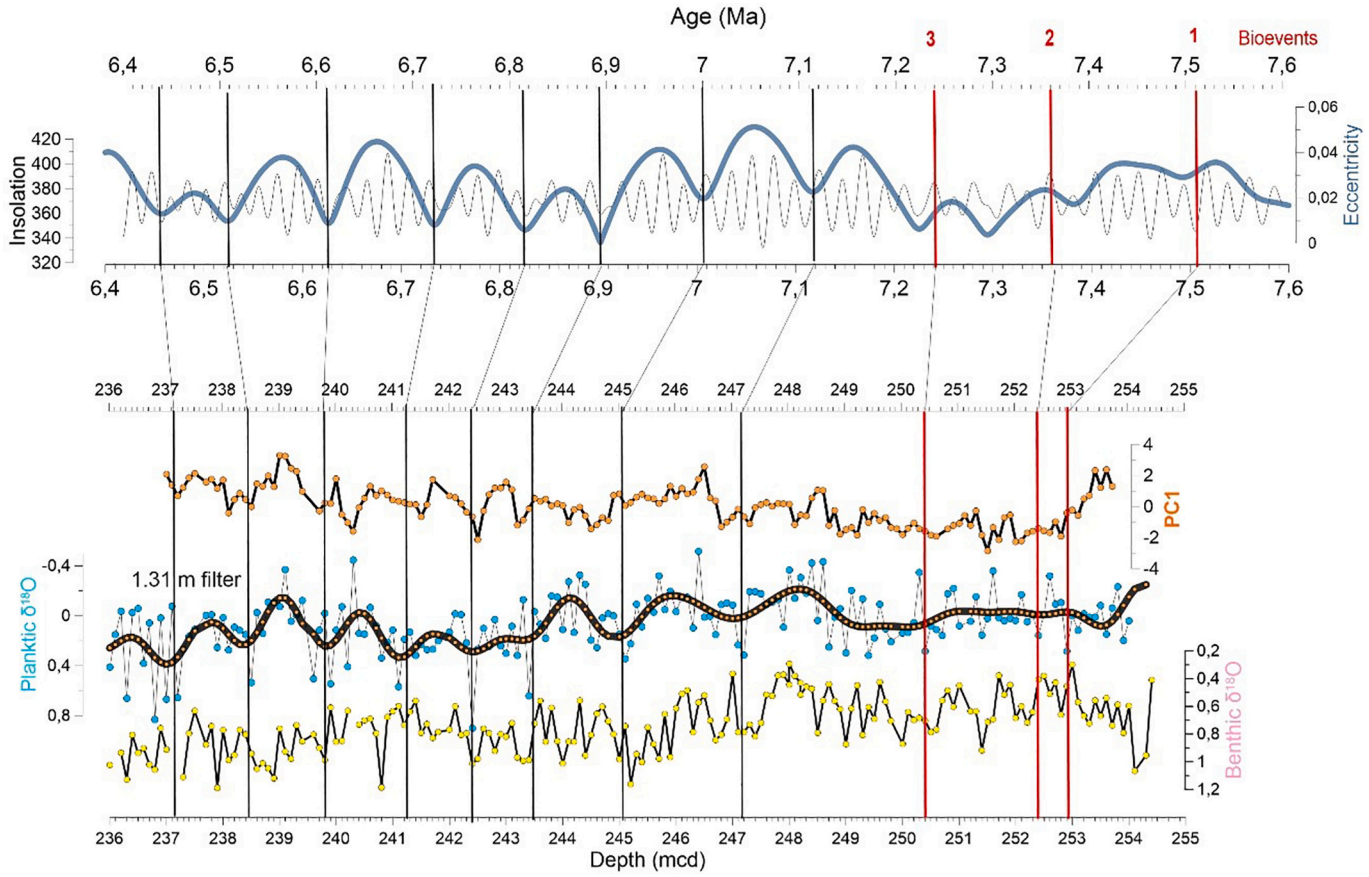

Fig. 10. Astronomical tuning of the lowermost interval of the Montemayor (7.6 to 6.4 Ma). Top: tuning target curves insolation and eccentricity (blue) from (Laskar et al., 2004). In the bottom, the PC1, planktic and benthic $\delta^{18}O$ records in depth domain (this study). The thick black curve represents the filtering of the planktic $\delta^{18}O$ record obtained with the higher power frequency. The vertical red lines show the main planktic foraminifer bioevents (Sierro et al., 1993, Lirer et al., 2019), while the black ones show the eccentricity minima phases. (For interpretation of the references to colour in this figure legend, the reader is referred to the web version of this article.)

composite in the Sorbas Basin that was the reference for GTS2004 and GTS2012 (Sierro et al., 2001). Some of the uncertainties related to the exact stratigraphic position of the magnetic polarity reversals in Sorbas can be due to the admittedly weak magnetic signal of the Abad section, which, for instance, did not allow the reliable recognition of Chron C3An (Sierro et al., 2001). Additionally, a delayed acquisition of the magnetic signal related with diagenetic processes cannot be excluded.

5. Discussion

Our new astronomically tuned late Tortonian – early Messinian stable isotope composite data of the Atlantic margin allows a detailed comparison of this record with other global and Mediterranean astronomically tuned isotope datasets. We focus here on the late Tortonian and early Messinian period, to better examine the effects of local vs. global climate changes, and the influence of Mediterranean waters on the Atlantic margin in a context of uplift and isolation of the Mediterranean basin from the global ocean that preconditioned the MSC (Bulian et al., 2022 and references therein). Such uplift and isolation were contemporaneous with the Late Miocene Carbon Isotope Shift (LMCIS; Hodell et al., 1994; Hodell et al., 2001; Hodell and Venz-Curtis, 2006).

5.1. Global vs. local changes in water masses

The Iberian Atlantic margin planktic $\delta^{18}O$ curve mimics the Atlantic 982 benthic record, i.e. see the peak at 7.07 Ma evident in both records and the good correspondence of the precession-driven cycles. This means that both the surface and deep waters of the GB recorded a strong global signal imprint.

Between 7.2 and 6.85 Ma, the global, North Atlantic, South China Sea, Mediterranean and Atlantic margin benthic $\delta^{18}O$ records show a subtle, but progressive trend towards heavier values, which is especially visible in the interglacial stages (Fig. 13). This long-term deep-water cooling trend probably reflects cooler Atlantic and Pacific deep waters or larger ice sheets in Antarctica or in the northern Hemisphere related with the Late Miocene Global Cooling (Herbert et al., 2016). Concordantly, in the South China Sea mixed layer isotope record (7.2 Ma), a slight increase in benthic $\delta^{18}O$ has been related with the progressive weakening of the summer monsoon in Southeast Asia during the LMCIS (Holbourn et al., 2021; Holbourn et al., 2018).

The comparison between different isotopic records reveals a 2 ‰ offset between the benthic $\delta^{18}O$ signal of the Atlantic margin, the Mediterranean, and the north Atlantic Site 982, most probably related to the temperature difference between cold Upper Northeast Atlantic Deep water (at the location of site 982) and the warmer MOW in the Atlantic margin (of Spain and Morocco). The Atlantic site registers a purely Atlantic deep cold-water signal, while the much shallower ones located in the GB contain a Mediterranean warm component as well. This temperature difference is visible today (Fig. 14), so that temperatures of around 4–5 °C are found at depth in Site 982 (1150 mbsl) whereas they reach 13 °C in the Gulf of Cadiz, influenced by the Mediterranean. Assuming a change of 0.23 ‰ per 1 °C, the 8–9 °C difference in temperature can explain the 2 ‰ offset between the two isotope records. Based on this we can assume that a Mediterranean signal was present along the Atlantic margins of Spain and Morocco also in the late Messinian.

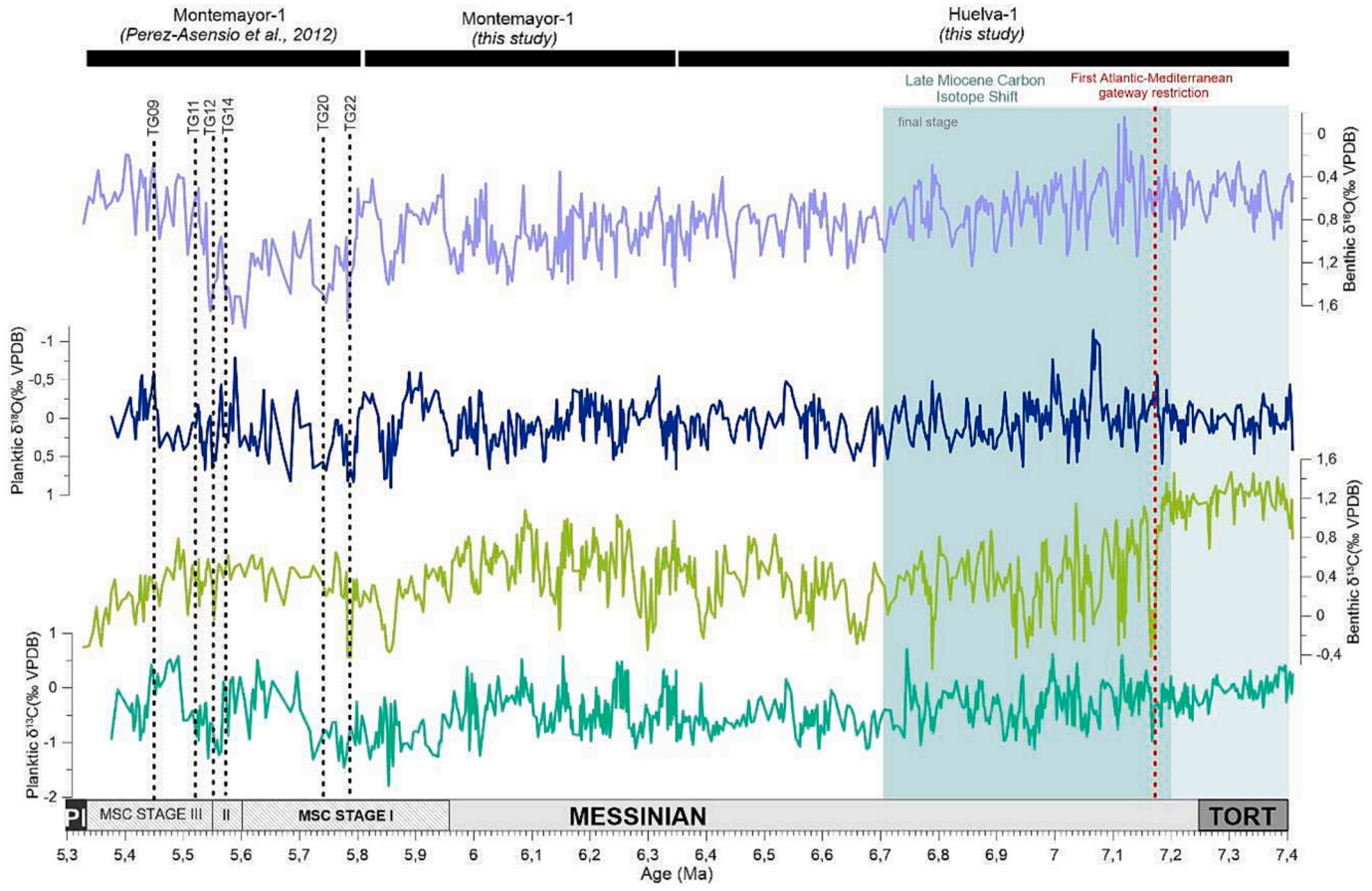

Fig. 11. Composite isotopic curve of the Iberian Atlantic margin showing planktic (*G. bulloides*) and benthic (*C. pachyderma*) foraminifer $\delta^{18}O$ and $\delta^{13}C$ records. The record from 7.4 until 6.36 Ma derives from Huelva (this study), the interval from 6.36 Ma to 5.8 Ma is covered by the Montemayor record (this study) as well as the topmost interval from 5.8 Ma until the base of the Pliocene (Pérez-Asensio et al., 2012a, 2012b). Glacial stages TG12, TG14, TG20 and TG22 and stages TG11 and TG9 (black dashed lines), the onset of the first Mediterranean-Atlantic gateway restriction (red dashed line), the Late Miocene Carbon isotope Shift (light blue shading) and its last more intense stage (darker blue shading) are put in for reference. (For interpretation of the references to colour in this figure legend, the reader is referred to the web version of this article.)

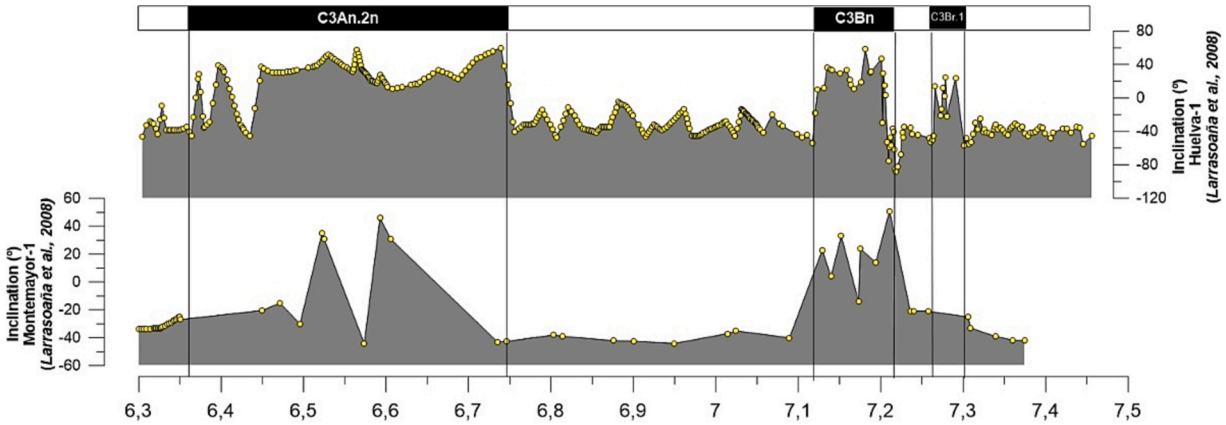

Fig. 12. Magnetic Inclination of the characteristic remanent magnetization inclination curves measured for the Huelva-1 and Montemayor-1 sites, plotted along with the inferred sequence of magnetozones (Larrasoaña et al., 2008). On top, the polarity is highlighted while the vertical lines indicate the new ages (also Table 2) for each identified Chrone.

Regarding the benthic $\delta^{13}C$ curve, the most noticeable change in the Iberian Atlantic margin is the prominent and abrupt drop observed at 7.17 Ma (Fig. 15), which is also visible, albeit with a smaller amplitude, in North Atlantic (Site 982) and South China Sea (Site 1146) records. During this time, from 7.5 and 5.5 Ma, coinciding in part with the global cooling (Herbert et al., 2016), the LMCIS took place at a global scale resulting in a decrease of approximately 1 ‰ of the global $\delta^{13}C$ of oceanic dissolved inorganic carbon ($\delta^{13}C_{DIC}$) (Hodell et al., 1994; Hodell et al., 2001; Hodell and Venz-Curtis, 2006; Holbourn et al., 2021). Contemporaneously, the same reduction in benthic $\delta^{13}C$ curve seems to be even more abrupt in the Mediterranean (Bulian et al., 2022), where it has been attributed to the start of the Mediterranean Atlantic gateway

Table 2
Ages of the Tortonian–Messinian chrons derived from the Huelva-1 and Montemayor-1 cores in this study. In addition, the table contains the astronomically calibrated ages of the chrons proposed by previous authors (Drury et al., 2017; Hilgen et al., 2012; Lourens et al., 2004; Sierro et al., 2001).

CHRONE	Astronomically calibrated age (Hilgen et al., 2012; Lourens et al., 2004; Sierro et al., 2001)	Astronomically calibrated age (Drury et al., 2017)	Astronomically calibrated age (This work)
T C3An.2n	6.43 Ma	6.39 Ma	6.37 Ma
B C3An.2n	6.73 Ma	6.73 Ma	6.75 Ma
T C3Bn	7.14 Ma	7.10 Ma	7.12 Ma
B C3Bn	7.21 Ma	7.21 Ma	7.22 Ma
T C3Br.1n	7.25 Ma	7.26 Ma	7.26 Ma
B C3Br.1n	7.28 Ma	7.30 Ma	7.30 Ma

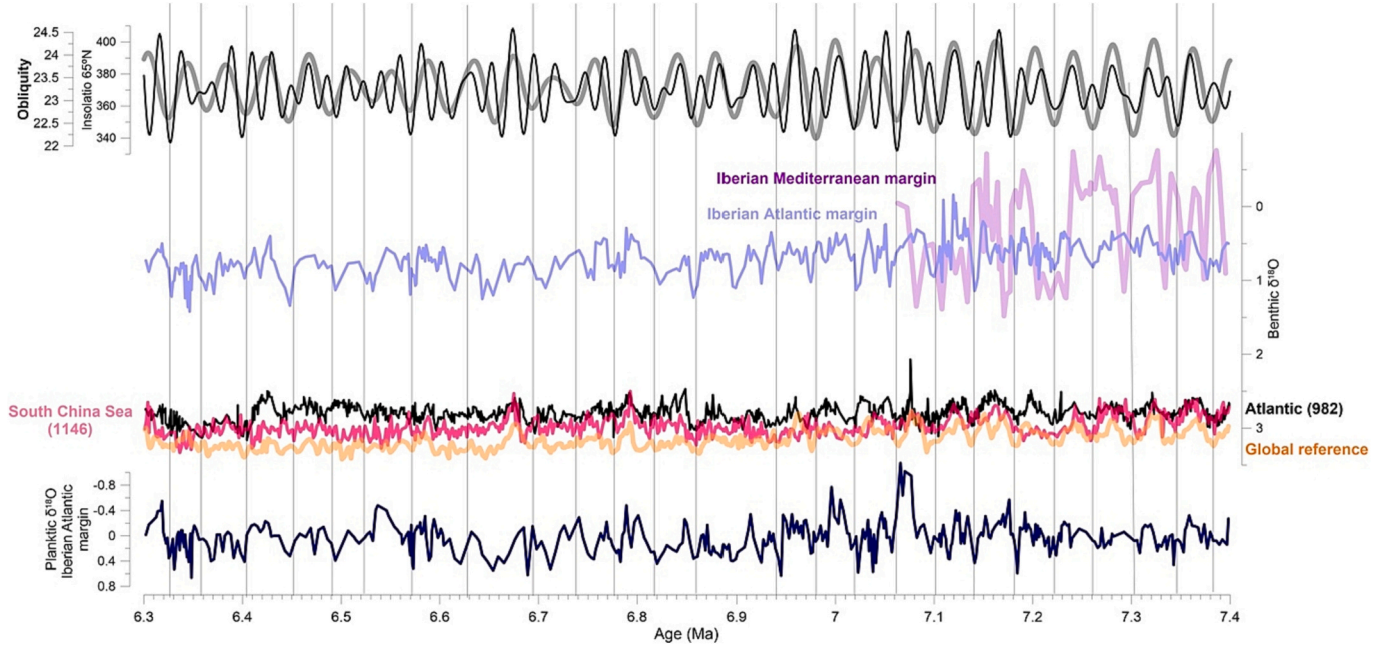

Fig. 13. Comparison between planktic $\delta^{18}O$ record of the Iberian Atlantic margin in dark blue (this study) and benthic $\delta^{18}O$ records including the Atlantic Iberian margin in light blue (this study), North Atlantic ODP Site 982 in black (Drury et al., 2018; Hodell et al., 2001), Alboran Basin (Iberian Mediterranean margin) Site 976 (Bulian et al., 2022) in violet, South China Sea Site 1146 (Holbourn et al., 2021; Holbourn et al., 2018) in pink and the global composite curve (Westerhold et al., 2020) in orange. To compare the absolute values of the curves, the isotope records that were measured on other benthic foraminifera species than the Atlantic margin composite were corrected according to their offset with respect to *C. pachyderma* reported in the literature. When the isotopic record was obtained measuring *C. wuellerstorfi* or *C. mundulus* (ODP sites 982) no correction has been applied because no offset has been found between these species and *C. pachyderma* (Hodell et al., 2001; Holbourn et al., 2007; Holbourn et al., 2018). The vertical lines indicate the minima of obliquity. (For interpretation of the references to colour in this figure legend, the reader is referred to the web version of this article.)

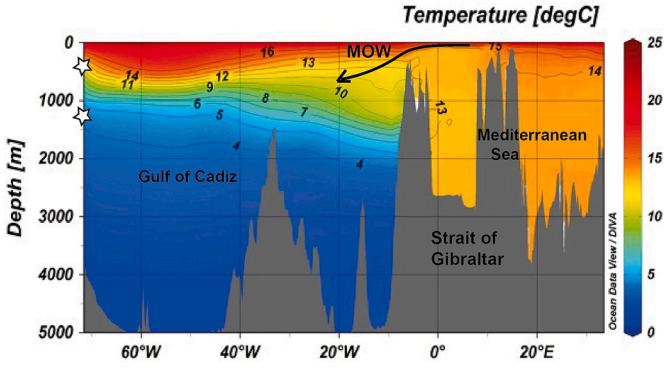

Fig. 14. Temperature profile showing the present-day Mediterranean Outflow Water (MOW) reaching the Gulf of Cadiz area (data from MedAtlas 2002-Database (Fichaut et al., 2003). The two stars show the possible paleodepth of the Montemayor-1\Huelva-1 (upper star) and Atlantic Site 982 (Hodell et al., 2001; Pérez-Asensio et al., 2014; lower star).

restriction and the concomitant reduction of Mediterranean deep-water renewal (Bulian et al., 2022; Bulian et al., 2021; Di Stefano et al., 2010; Kouwenhoven et al., 1999; Kouwenhoven et al., 2003; Kouwenhoven and Van der Zwaan, 2006; Seidenkrantz et al., 2000). Before 7.17 Ma, high benthic $\delta^{13}C$ in the deep Mediterranean and the Atlantic margin of Spain, indicate good bottom water ventilation on both sides of the ancient paleostraits, similar to that recorded in the intermediate to deep North Atlantic. However, at 7.17 Ma, a drastic and pronounced drop in benthic $\delta^{13}C$ reflects a sudden presence of poor ventilated bottom waters in the Mediterranean and the Atlantic margin of Spain, while the open Atlantic site remained well ventilated during the Messinian.

We interpret that the sudden drop in ventilation occurring in the deep Mediterranean in response to uplift of the paleostraits of the Gibraltar Arch, and the consequent restriction of the Atlantic-Mediterranean water exchange, was transmitted to the Atlantic margin through the MOW, although the influence of these poorly ventilated waters never reached the open Atlantic.

The benthic $\delta^{13}C$ record in the Atlantic margin of Spain displays some cyclicity that seems to be in phase with the Mediterranean carbon isotope record, and the $\delta^{13}C$ negative peaks of the two records are linked to both insolation and obliquity maxima. In Fig. 15, the vertical lines

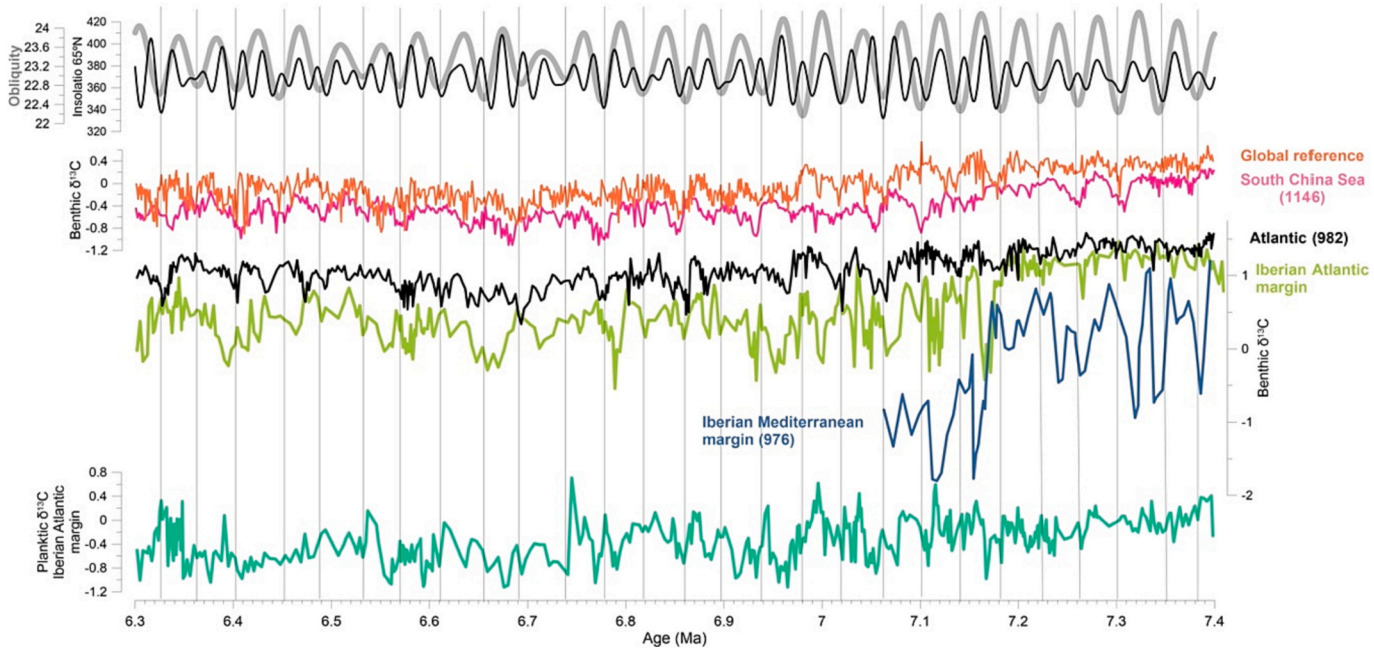

Fig. 15. Comparison between planktic $\delta^{13}C$ record of Iberian Atlantic margin in dark green (this study) and benthic $\delta^{13}C$ records including the Iberian Atlantic margin composite in light green (this study), North Atlantic ODP Site 982 in black (Drury et al., 2018; Hodell et al., 2001), Alboran Basin (Iberian Mediterranean margin) Site 976 (Bulian et al., 2022) in blue, South China Sea Site 1146 (Holbourn et al., 2021; Holbourn et al., 2018) in pink and the global curve (Westerhold et al., 2020) in orange. To compare the absolute values of the curves, the isotope records that were measured on other benthic foraminifer species than the GB composite were corrected according to their offset with respect to *C. pachyderma* reported in the literature. When the isotopic record was obtained measuring *C. wuellerstorfi* or *C. mundulus* (ODP sites 982) no correction has been applied because no offset has been found between these species and *C. pachyderma* (Hodell et al., 2001; Holbourn et al., 2007; Holbourn et al., 2018). The vertical lines indicate the minima of obliquity. (For interpretation of the references to colour in this figure legend, the reader is referred to the web version of this article.)

highlight the obliquity minima phases. On the contrary, the global isotope record shows an out of phase trend in respect to the GB and the Mediterranean. As already pointed out by Bulian et al. (2022), the benthic $\delta^{13}C$ from ODP Site 1146 and Site 982 follows a global pattern of lower benthic $\delta^{13}C$ during glacial periods (higher benthic $\delta^{18}O$) during obliquity minima, probably due to a greater CO_2 storage in the deep ocean (Holbourn et al., 2018). By contrast, the Mediterranean benthic $\delta^{13}C$ cyclicity is controlled by northern hemisphere summer insolation, with lower benthic $\delta^{13}C$ values recorded during summer insolation maxima at times of sapropel formation. This means that the open ocean stable isotope signals are dominated by obliquity, while the Mediterranean Sea and the GB records are modulated by precession. This has been confirmed by Drury et al. (2017), who highlights how in equatorial Pacific site U1337, especially after 7.2 Ma, the obliquity forcing overshadows the influence of precession.

5.2. Mediterranean water influence on the Atlantic margin

Considering that the MOW today reaches the Gulf of Cadiz as an intermediate water mass along the south-western Iberian margin (e.g., Hernandez-Molina et al., 2014), the same probably occurred during the late Miocene at the location of Huelva and Montemayor, implying that the Mediterranean outflow was probably flowing along this margin, transporting into the Atlantic the changes that have occurred in the Mediterranean (i.e., Bulian et al., 2022; Bulian et al., 2021). Consequently, a restriction of the Mediterranean-Atlantic gateways would mean the presence of a larger proportion of Atlantic cold intermediate water replacing the warmer Mediterranean outflow. This would have reduced the bottom water temperature and thus increased the benthic foraminifer $\delta^{18}O$ values. In more recent times, Voelker et al. (2006), Sierro et al. (2020) and Raddatz et al. (2011), have reported how the benthic $\delta^{13}C$ signal of the Gulf of Cadiz in the Pleistocene mainly reflects the chemical properties of the MOW and Mediterranean deep water, and, therefore, the higher or lower residence time of the deep water within the Mediterranean. This would imply how a decrease in Mediterranean $\delta^{13}C$ would be seen on the Atlantic side of the gateway as well.

In the Iberian Atlantic margin, together with the benthic $\delta^{13}C$ drop at 7.17 Ma a change in the amplitude of the benthic carbon isotope cyclicity is also visible. Before the event, the benthic $\delta^{13}C$ is highly stable and does not show major oscillations, but afterwards a big amplitude fluctuation starts. We also observe how the lower $\delta^{13}C$ values in the Iberian Atlantic margin bathed by the MOW seem to reflect the Mediterranean deoxygenation events as highlighted by Sierro et al. (2020) for the last 250 kyr of Gulf of Cadiz at Site U1389. With small offsets in some cases, probably due to inaccuracies in the tuning of PC1 with insolation, the events of lower benthic $\delta^{13}C$ recorded in the Iberian Atlantic margin are correlated with sapropel events in the Eastern Mediterranean (Faneromeni section Cycles 18–29) and with analogous lows in the Western Mediterranean isotope records (Bulian et al., 2022). In addition, the interference pattern between obliquity and precession reflected by the interbedding of prominent and weak sapropels seen in Faneromeni in the first sapropels is also visible in the benthic $\delta^{13}C$ of the Iberian Atlantic margin (Fig. 16). A recent study performed on Site U1389, located in the main descending core of the MOW in the Gulf of Cadiz, shows how beds with low sand percentages are linked with periods of weak MOW and lighter benthic $\delta^{13}C$ values corresponding with phases of sapropel deposition in the Mediterranean (Sierro et al., 2020). The higher and more stable benthic $\delta^{13}C$ values recorded in the Iberian Margin prior to 7.17 Ma reflects the higher $\delta^{13}C$ of Mediterranean deep waters because of the continuous and intense deep-water ventilation during the latest Tortonian and earliest Messinian, before the onset of the Atlantic-Mediterranean restriction. The more accentuated cyclical pattern observed in the Iberian Atlantic margin stable isotope record after 7.17 Ma could have therefore been caused by a higher contrast in the MOW between the wet and the dry phase, related with an increase in the sensitivity of the restricted Mediterranean basin to climate change

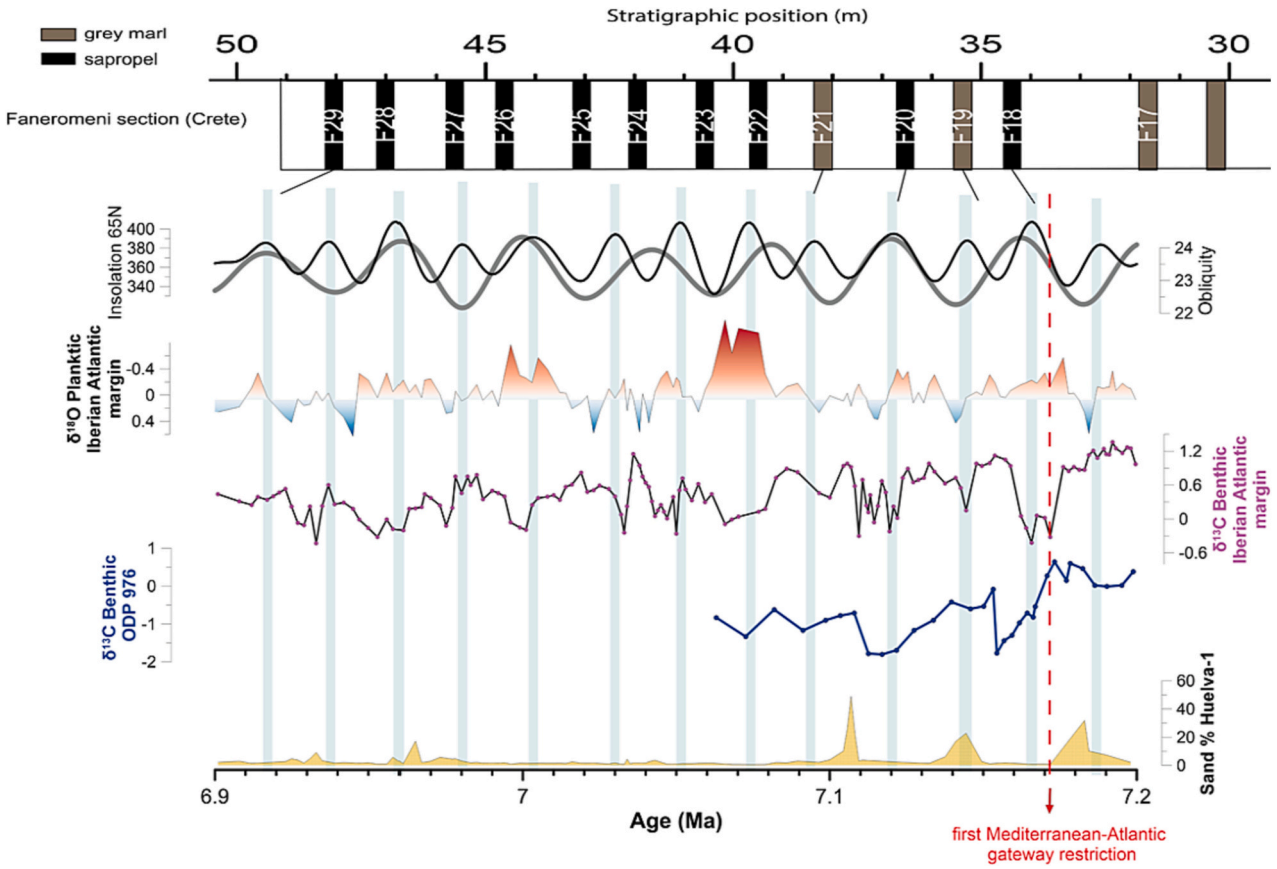

Fig. 16. From top to bottom: simplified stratigraphic log of the Faneromeni section (Krijgsman et al., 1994; Santarelli et al., 1998) showing sapropels and marly layers; insolation curve (black) and the obliquity curve (grey) from Laskar et al. (2004); planktic $\delta^{18}O$ records of the Iberian Atlantic margin composite section (this work); benthic $\delta^{13}C$ records of the Iberian Atlantic margin composite section (this wok) and the benthic $\delta^{13}C$ records of ODP Site 976. The vertical blue shading highlights the insolation cycles. (For interpretation of the references to colour in this figure legend, the reader is referred to the web version of this article.)

(Bulian et al., 2021).

Between 7.2 and 7.1 Ma, three sand layers were identified in Huelva. These levels, characterized by sand contents as high as 50% (Fig. 16) are clearly linked to phases of obliquity minima and therefore colder, glacial climates characterized by lower sea level. These sand layers could be caused by turbidity deposition triggered by global eustatic sea level drops and/or by MOW intensification during colder conditions (de Castro et al., 2021). Additional sedimentological information is required in order to discard if these sandy layers correspond to contourites or turbidites.

Consequently, it can be assumed that apart from a global signal and even if the connection between the GB and Mediterranean diminished, the MOW was still reaching the two sites in the Atlantic margin, contributing for the bigger part to their deep-water signature. Considering that the benthic $\delta^{13}C$ in the Atlantic margin seems to mimic the records of Mediterranean ventilation at least until 7.06 Ma, we can assume that until then the MOW reached the Atlantic margin of Spain. The obtained data allow to constrain the period of activity of the MOW into the Atlantic which has been demonstrated to play a major role in the North Atlantic surface temperatures (Potter and Lozier, 2004). In this sense, weak and even "free-MOW" conditions could be linked with the moment when East Greenland glaciers reached the coast at ~7.3 Ma and when periodic Ice Rafted Debris become common to date at site ODP 918 (Bierman et al., 2016; John and Krissek, 2002) as previously suggested (Capella et al., 2019). A new continuous record from the Mediterranean would be necessary to trace the moment when less water was reaching the GB through the Gateways of the Gibraltar Arch. Following the same reasoning we can assume that the poorly ventilated MOW was present in the GB for most of the early Messinian as may be inferred from the overall low benthic $\delta^{13}C$ compared with the highly ventilated bottom waters in the deep north Atlantic. Similar observations have been previously made for both the Western and Eastern Mediterranean (i.e., Bulian et al., 2022; Kouwenhoven et al., 2003). New, deeper water isotope records in the Atlantic margin are necessary to confirm this hypothesis and exclude the possible occurrence of lower benthic $\delta^{13}C$ values in Huelva and Montemayor in response to a local shallowing of the basin and the existence of shallower waters closer to the oxygen minimum zone, which are typically more depleted in ^{13}C.

6. Conclusion

The newly acquired stable isotope and elemental data from the lower interval of Montemayor-1 (257.3–236 md = 8–6.37 Ma) and Huelva-1 (170–120 md = 7.4–6.3 Ma) cores enabled a high-resolution astronomical tuning and the production of a new Iberian Atlantic margin composite isotopic record from the late Tortonian to early Pliocene. Additionally, the new chronology allowed to compare the timing of the magnetic reversals recorded in these sites during the Messinian with the ages of these magnetic reversals in other locations. Overall, a long-term increase in the benthic $\delta^{18}O$ is observed, probably reflecting the global gradual cooling recorded during the Messinian.

Based on the new chronology, the events of increase of bottom water residence time, temperature and salinity registered in the GB at 7.17 Ma are contemporaneous with changes reported from numerous Mediterranean locations (Bulian et al., 2021; Di Stefano et al., 2010; e.g., Kouwenhoven et al., 1999; Kouwenhoven et al., 2003; Kouwenhoven and Van der Zwaan, 2006; Seidenkrantz et al., 2000). The high benthic $\delta^{13}C$ recorded in the Atlantic Iberian margin before 7.17 Ma and the

sudden and high amplitude drop observed at this time probably reflects the drastic changes occurring in the Mediterranean in response to its isolation from the Atlantic. The high benthic $\delta^{13}C$ in the latest Tortonian earliest Messinian was the result of intense and continuous, Mediterranean deep-water ventilation that was drastically reduced at 7.17 Ma because of water exchange restriction with the Atlantic. This chemical signature was transported to the Atlantic through the MOW even though the Gibraltar gateways were largely reduced at that time.

The presence of MOW in the Atlantic Iberian Margin of Spain is also visible in the benthic $\delta^{13}C$ after 7.17 Ma. The observation of precession driven drops in benthic $\delta^{13}C$ seems to reflect the events of poor-bottom water ventilation in the Mediterranean during sapropel deposition. This cyclical pattern of the benthic $\delta^{13}C$ in the Atlantic margin of Spain is different from that recorded in the open Atlantic and Pacific, where benthic $\delta^{13}C$ variability follows glacial cycles in phase with obliquity.

The comparison of the benthic $\delta^{18}O$ records in the Atlantic margin of Spain and ODP site 982 in intermediate depths of the North Atlantic shows a continuous $\delta^{18}O$ difference of near 2 units along the Messinian. This difference, which was probably the result of the presence of warmer waters near the Gibraltar Arch paleostraits, seems to suggest the continuous flow of Mediterranean warm water to the Atlantic throughout the Messinian.

CRediT authorship contribution statement

Francesca Bulian: Conceptualization, Investigation, Methodology, Data curation, Writing – original draft. **Francisco J. Jiménez-Espejo:** Conceptualization, Supervision, Writing – review & editing. **Nils Andersen:** Formal analysis, Writing – review & editing. **Juan C. Larrasoaña:** Resources, Writing – review & editing. **Francisco J. Sierro:** Conceptualization, Methodology, Data curation, Supervision, Writing – review & editing.

Declaration of Competing Interest

The authors declare that they have no known competing financial interests or personal relationships that could have appeared to influence the work reported in this paper.

Data availability

Data will be made available on request.

Acknowledgments

The authors appreciate the work of Jose Ignacio Martin Cruz in sample processing and preparation. All fellow ESRs and supervisors from the SALTGIANT project are thanked for their valuable suggestions and discussions. We would also like to thank Nucleus, in particular the Area of Instrumental Techniques, X-ray Diffraction team of Salamanca University that performed the X-ray geochemical analyses on our samples. This research has received funding from the European Union's Horizon 2020 research and innovation program under the Marie Skłodowska-Curie grant agreement n° 765256 SALTGIANT. Funding from the Spanish Ministry of Universities and Research, project PID2021-128322NB-I00, is also acknowledged. Two anonymous reviewers are also acknowledged for their useful comments.

References

Abdi, H., Williams, L.J., 2010. Principal component analysis. Wiley Interdisciplinary Rev. Computat. Stat. 2 (4), 433–459.
Aguirre, J., 1992. Evolución de las asociaciones fósiled del Plioceno meeino de Cabo de Roche (Cadiz). Rev. española de paleontología 3, 3–10.
Bahr, A., Kaboth, S., Jiménez-Espejo, F., Sierro, F., Voelker, A., Lourens, L., Röhl, U., Reichart, G., Escutia, C., Hernández-Molina, F., 2015. Persistent monsoonal forcing of Mediterranean outflow water dynamics during the late Pleistocene. Geology 43 (11), 951–954.
Benson, R.H., Rakic-El Bied, K., Bonaduce, G., 1991. An important current reversal (influx) in the Rifian Corridor (Morocco) at the Tortonian-Messinian boundary: the end of Tethys Ocean. Paleoceanography 6 (1), 165–192.
Berástegui, X., Banks, C., Puig, C., Taberner, C., Waltham, D., Fernández, M., 1998. Lateral diapiric emplacement of Triassic evaporites at the southern margin of the Guadalquivir Basin, Spain. Geol. Soc. Lond., Spec. Publ. 134 (1), 49–68.
Betzler, C., Braga, J.C., Martín, J.M., Sanchez-Almazo, I.M., Lindhorst, S., 2006. Closure of a seaway: stratigraphic record and facies (Guadix basin, Southern Spain). Int. J. Earth Sci. 95 (5), 903–910.
Bialik, O.M., Frank, M., Betzler, C., Zammit, R., Waldmann, N.D., 2019. Two-step closure of the Miocene Indian ocean gateway to the Mediterranean. Sci. Rep. 9 (1), 1–10.
Bierman, P.R., Shakun, J.D., Corbett, L.B., Zimmerman, S.R., Rood, D.H., 2016. A persistent and dynamic East Greenland Ice Sheet over the past 7.5 million years. Nature 540 (7632), 256–260.
Blanc, P.-L., 2002. The opening of the Plio-Quaternary Gibraltar Strait: assessing the size of a cataclysm. Geodin. Acta 15 (5–6), 303–317.
Bulian, F., Sierro, F.J., Ledesma, S., Jiménez-Espejo, F.J., Bassetti, M.-A., 2021. Messinian West Alboran Sea record in the proximity of Gibraltar: Early signs of Atlantic-Mediterranean gateway restriction. Mar. Geol. 106430.
Bulian, F., Kouwenhoven, T.J., Jiménez-Espejo, F.J., Krijgsman, W., Andersen, N., Sierro, F.J., 2022. Impact of the Mediterranean-Atlantic connectivity and the late Miocene carbon shift on deep-sea communities in the Western Alboran Basin. Palaeogeogr. Palaeoclimatol. Palaeoecol. 110841.
Capella, W., Hernández-Molina, F.-J., Flecker, R., Hilgen, F., Hssain, M., Kouwenhoven, T., van Oorschot, M., Sierro, F., Stow, D., Trabucho-Alexandre, J., 2017. Sandy contourite drift in the late Miocene Rifian Corridor (Morocco): reconstruction of depositional environments in a foreland-basin seaway. Sediment. Geol. 355, 31–57.
Capella, W., Barhoun, N., Flecker, R., Hilgen, F., Kouwenhoven, T., Matenco, L., Sierro, F. J., Tulbure, M., Yousfi, M.Z., Krijgsman, W., 2018. Palaeogeographic evolution of the late Miocene Rifian Corridor (Morocco): reconstructions from surface and subsurface data. Earth Sci. Rev. 180, 37–59.
Capella, W., Flecker, R., Hernández-Molina, F.J., Simon, D., Meijer, P.T., Rogerson, M., Sierro, F.J., Krijgsman, W., 2019. Mediterranean isolation preconditioning the Earth System for late Miocene climate cooling. Sci. Rep. 9 (1).
Capella, W., Spakman, W., van Hinsbergen, D.J., Chertova, M.V., Krijgsman, W., 2020. Mantle resistance against Gibraltar slab dragging as a key cause of the Messinian Salinity Crisis. Terra Nova 32 (2), 141–150.
Carrapa, B., Clementz, M., Feng, R., 2019. Ecological and hydroclimate responses to strengthening of the Hadley circulation in South America during the Late Miocene cooling. Proc. Natl. Acad. Sci. 116 (20), 9747–9752.
Christensen, B.A., De Vleeschouwer, D., Henderiks, J., Groeneveld, J., Auer, G., Drury, A. J., Karatsolis, B.T., Lyu, J., Betzler, C., Eberli, G.P., 2021. Late miocene onset of tasman leakage and southern hemisphere supergyre ushers in near-modern circulation. Geophys. Res. Lett. 48 (18) e2021GL095036.
CIESM, 2008. The Messinian salinity crisis from mega-deposits to microbiology. In: Briand, F. (Ed.), A consensus report, in 33ème CIESM Workshop Monographs, 33. CIESM, 16, bd de Suisse, MC-98000, Monaco, pp. 1–168.
Corbí, H., Lancis, C., García-García, F., Pina, J.-A., Soria, J.M., Tent-Manclús, J.E., Viseras, C., 2012. Updating the marine biostratigraphy of the Granada Basin (central Betic Cordillera). Insight for the Late Miocene palaeogeographic evolution of the Atlantic–Mediterranean seaway. Geobios 45 (3), 249–263.
Di Stefano, A., Verducci, M., Lirer, F., Ferraro, L., Iaccarino, S.M., Hüsing, S.K., Hilgen, F. J., 2010. Paleoenvironmental conditions preceding the Messinian Salinity Crisis in the Central Mediterranean: integrated data from the Upper Miocene Trave section (Italy). Palaeogeogr. Palaeoclimatol. Palaeoecol. 297 (1), 37–53.
Drury, A.J., Westerhold, T., Frederichs, T., Tian, J., Wilkens, R., Channell, J.E., Evans, H., John, C.M., Lyle, M., Röhl, U., 2017. Late Miocene climate and time scale reconciliation: Accurate orbital calibration from a deep-sea perspective. Earth Planet. Sci. Lett. 475, 254–266.
Drury, A.J., Westerhold, T., Hodell, D., Röhl, U., 2018. Reinforcing the North Atlantic backbone: revision and extension of the composite splice at ODP Site 982. Clim. Past 14 (3), 321–338.
Fadil, A., Vernant, P., McClusky, S., Reilinger, R., Gomez, F., Ben Sari, D., Mourabit, T., Feigl, K., Barazangi, M., 2006. Active tectonics of the western Mediterranean: Geodetic evidence for rollback of a delaminated subcontinental lithospheric slab beneath the Rif Mountains, Morocco. Geology 34 (7), 529–532.
Fichaut, M., Garcia, M., Giorgetti, A., Iona, A., Kuznetsov, A., Rixen, M., Group, M, 2003. MEDAR/MEDATLAS 2002: A Mediterranean and Black Sea database for operational oceanography. In: Elsevier Oceanography Series. Elsevier, pp. 645–648.
Flecker, R., Krijgsman, W., Capella, W., De Castro Martíns, C., Dmitrieva, E., Mayser, J. P., Marzocchi, A., Modestou, S., Ochoa, D., Simon, D., Tulbure, M., Van Den Berg, B., Van Der Schee, M., De Lange, G., Ellam, R., Govers, R., Gutjahr, M., Hilgen, F., Kouwenhoven, T., Lofi, J., Meijer, P., Sierro, F.J., Bachiri, N., Barhoun, N., Alami, A. C., Chacon, B., Flores, J.A., Gregory, J., Howard, J., Lunt, D., Ochoa, M., Pancost, R., Vincent, S., Yousfi, M.Z., 2015. Evolution of the Late Miocene Mediterranean–Atlantic gateways and their impact on regional and global environmental change. Earth Sci. Rev. 150, 365–392.
Garcia-Castellanos, D., Villaseñor, A., 2011. Messinian salinity crisis regulated by competing tectonics and erosion at the Gibraltar arc. Nature 480 (7377), 359.
Garcia-Castellanos, D., Fernandez, M., Torné, M., 2002. Modeling the evolution of the Guadalquivir foreland basin (southern Spain). Tectonics 21 (3), 9–1–9-17.

Garcia-Castellanos, D., Estrada, F., Jiménez-Munt, I., Gorini, C., Fernández, M., Vergés, J., De Vicente, R., 2009. Catastrophic flood of the Mediterranean after the Messinian salinity crisis. Nature 462 (7274), 778.
Garcia-Castellanos, D., Micallef, A., Estrada, F., Camerlenghi, A., Ercilla, G., Periáñez, R., Abril, J.M., 2019. The Zanclean megaflood of the Mediterranean–Searching for additional evidence. Earth Sci. Rev. 103061.
González-Delgado, J.A., Civis, J., Dabrio, C.J., Goy, J.L., Ledesma, S., Pais, J., 2004. Cuenca del Guadalquivir. In: Vera, J.A. (Ed.), Geología de España. SGE-IGME, Madrid, pp. 543–550.
Hammer, Ø., Harper, D.A., Ryan, P.D., 2001. PAST: paleontological statistics software package for education and data analysis. Palaeontol. Electron. 4 (1), 9.
Herbert, T.D., Lawrence, K.T., Tzanova, A., Peterson, L.C., Caballero-Gill, R., Kelly, C.S., 2016. Late Miocene global cooling and the rise of modern ecosystems. Nat. Geosci. 9 (11), 843–847.
Hernandez-Molina, F.J., Stow, D.A.V., Alvarez-Zarikian, C.A., Acton, G., Bahr, A., Balestra, B., Ducassou, E., Flood, R., Flores, J.A., Furota, S., Grunert, P., Hodell, D., Jimenez-Espejo, F., Kim, J.K., Krissek, L., Kuroda, J., Li, B., Llave, E., Lofi, J., Lourens, L., Miller, M., Nanayama, F., Nishida, N., Richter, C., Roque, C., Pereira, H., Sanchez Goni, M.F., Sierro, F.J., Singh, A.D., Sloss, C., Takashimizu, Y., Tzanova, A., Voelker, A., Williams, T., Xuan, C., 2014. Onset of Mediterranean outflow into the North Atlantic, 344 (6189), 1244–1250.
Hilgen and Krijgsman, 1999. Cyclostratigraphy and astrochronology of the Tripoli diatomite formation (pre-evaporite Messinian, Sicily, Italy). Terra Nova 11 (1), 16–22.
Hilgen, F., Bissoli, L., Iaccarino, S., Krijgsman, W., Meijer, R., Negri, A., Villa, G., 2000a. Integrated stratigraphy and astrochronology of the Messinian GSSP at Oued Akrech (Atlantic Morocco). Earth Planet. Sci. Lett. 182 (3–4), 237–251.
Hilgen, F., Iaccarino, S., Krijgsman, W., Villa, G., Langereis, C., Zachariasse, W., 2000b. The global boundary stratotype section and point (GSSP) of the Messinian Stage (uppermost Miocene). Episodes 23 (3), 172–178.
Hilgen, F., Lourens, L., van Dam, J.A., 2012. The neogene period.
Hodell, D.A., Venz-Curtis, K.A., 2006. Late Neogene history of deepwater ventilation in the Southern Ocean. Geochem. Geophys. Geosyst. 7 (9).
Hodell, D.A., Benson, R.H., Kent, D.V., Boersma, A., Rakic-El Bied, K., 1994. Magnetostratigraphic, biostratigraphic, and stable isotope stratigraphy of an Upper Miocene drill core from the Salé Briqueterie (northwestern Morocco): A high-resolution chronology for the Messinian stage. Paleoceanography 9 (6), 835–855.
Hodell, D.A., Curtis, J.H., Sierro, F.J., Raymo, M.E., 2001. Correlation of late Miocene to early Pliocene sequences between the Mediterranean and North Atlantic. Paleoceanography 16 (2), 164–178.
Holbourn, A., Kuhnt, W., Schulz, M., Flores, J.-A., Andersen, N., 2007. Orbitally-paced climate evolution during the middle Miocene "Monterey" carbon-isotope excursion. Earth Planet. Sci. Lett. 261 (3–4), 534–550.
Holbourn, A.E., Kuhnt, W., Clemens, S.C., Kochhann, K.G., Jöhnck, J., Lübbers, J., Andersen, N., 2018. Late Miocene climate cooling and intensification of southeast Asian winter monsoon. Nat. Commun. 9 (1), 1–13.
Holbourn, A., Kuhnt, W., Clemens, S.C., Heslop, D., 2021. A~ 12 Myr Miocene Record of East Asian Monsoon variability from the South China Sea. Paleoceanogr. Paleoclimatol. 36 (7) e2021PA004267.
Hsü, K.J., Ryan, W.B.F., Cita, M.B., 1973. Late miocene desiccation of the mediterranean. Nature 242 (5395), 240–244.
Hüsing, S., Kuiper, K., Link, W., Hilgen, F.J., Krijgsman, W., 2009. The upper Tortonian–lower Messinian at Monte dei Corvi (Northern Apennines, Italy): completing a Mediterranean reference section for the Tortonian stage. Earth Planet. Sci. Lett. 282 (1–4), 140–157.
Hüsing, S., Oms, O., Agustí, J., Garcés, M., Kouwenhoven, T., Krijgsman, W., Zachariasse, W.-J., 2010. On the late Miocene closure of the Mediterranean–Atlantic gateway through the Guadix basin (southern Spain). Palaeogeogr. Palaeoclimatol. Palaeoecol. 291 (3–4), 167–179.
Jiménez-Moreno, G., Pérez-Asensio, J.N., Larrasoaña, J.C., Aguirre, J., Civis, J., Rivas-Carballo, M.R., Valle-Hernández, M.F., González-Delgado, J.A., 2013. Vegetation, sea-level, and climate changes during the Messinian salinity crisis. Bulletin 125 (3–4), 432–444.
John, K.E.S., Krissek, L.A., 2002. The late Miocene to Pleistocene ice-rafting history of southeast Greenland. Boreas 31 (1), 28–35.
Jöhnck, J., Kuhnt, W., Holbourn, A., Andersen, N., 2020. Variability of the Indian Monsoon in the Andaman Sea across the Miocene-Pliocene transition. Paleoceanogr. Paleoclimatol. 35 (9) e2020PA003923.
Kaboth, S., de Boer, B., Bahr, A., Zeeden, C., Lourens, L.J., 2017. Mediterranean Outflow Water dynamics during the past~ 570 kyr: Regional and global implications. Paleoceanography 32 (6), 634–647.
Kaboth-Bahr, S., Bahr, A., Stepanek, C., Catunda, M.C.A., Karas, C., Ziegler, M., García-Gallardo, Á., Grunert, P., 2021. Mediterranean heat injection to the North Atlantic delayed the intensification of Northern Hemisphere glaciations. Communicat. Earth & Environ. 2 (1), 158.
Kouwenhoven, T.J., 2000. Survival Under Stress: Benthic Foraminiferal Patterns and Cenozoic Biotic Crises. Faculteit Aardwetenschappen.
Kouwenhoven, T.V., Van der Zwaan, G., 2006. A reconstruction of late Miocene Mediterranean circulation patterns using benthic foraminifera. Palaeogeogr. Palaeoclimatol. Palaeoecol. 238 (1–4), 373–385.
Kouwenhoven, T., Seidenkrantz, M.-S., Van der Zwaan, G., 1999. Deep-water changes: the near-synchronous disappearance of a group of benthic foraminifera from the Late Miocene Mediterranean. Palaeogeogr. Palaeoclimatol. Palaeoecol. 152 (3–4), 259–281.
Kouwenhoven, T.J., Hilgen, F.J., Van Der Zwaan, G.J., 2003. Late Tortonian–early Messinian stepwise disruption of the Mediterranean–Atlantic connections: constraints from benthic foraminiferal and geochemical data. Palaeogeogr. Palaeoclimatol. Palaeoecol. 198 (3–4), 303–319.
Krijgsman, W., Langereis, C., 2000. Magnetostratigraphy of the Zobzit and Koudiat Zarga sections (Taza-Guercif basin, Morocco): implications for the evolution of the Rifian Corridor. Mar. Pet. Geol. 17 (3), 359–371.
Krijgsman, W., Hilgen, F., Langereis, C., Zachariasse, W., 1994. The age of the Tortonian/Messinian boundary. Earth Planet. Sci. Lett. 121, 533–547.
Krijgsman, W., Hilgen, F., Raffi, I., Sierro, F.J., Wilson, D., 1999a. Chronology, causes and progression of the Messinian salinity crisis. Nature 400 (6745), 652.
Krijgsman, W., Langereis, C., Zachariasse, W., Boccaletti, M., Moratti, G., Gelati, R., Iaccarino, S., Papani, G., Villa, G., 1999b. Late Neogene evolution of the Taza–Guercif Basin (Rifian Corridor, Morocco) and implications for the Messinian salinity crisis. Mar. Geol. 153 (1–4), 147–160.
Krijgsman, W., Capella, W., Simon, D., Hilgen, F.J., Kouwenhoven, T.J., Meijer, P.T., Sierro, F.J., Tulbure, M.A., van den Berg, B.C., van der Schee, M., 2018. The Gibraltar corridor: watergate of the messinian salinity crisis. Mar. Geol. 403, 238–246.
Larrasoaña, J., González-Delgado, J., Civis, J., Sierro, F., Alonso-Gavilán, G., Pais, J., 2008. Magnetobiostratigraphic dating and environmental magnetism of Late Neogene marine sediments recovered at the Huelva-1 and Montemayor-1 boreholes (lower Guadalquivir basin, Spain). Geo-Temas 10, 1175–1178.
Larrasoaña, J.C., Liu, Q., Hu, P., Roberts, A.P., Mata, P., Civis, J., Sierro, F.J., Pérez-Asensio, J.N., 2014. Paleomagnetic and paleoenvironmental implications of magnetofossil occurrences in late Miocene marine sediments from the Guadalquivir Basin, SW Spain. Front. Microbiol. 5, 71.
Laskar, J., Robutel, P., Joutel, F., Gastineau, M., Correia, A., Levrard, B., 2004. A long-term numerical solution for the insolation quantities of the Earth. Astron. Astrophys. 428 (1), 261–285.
Ledesma, S., 2000. Astrobiocronología y estratigrafía de alta resolución del Neógeno de la Cuenca del Guadalquivir- Golfo de Cádiz. PhD thesis,. Universidad de Salamanca, p. 464.
Lirer, F., Foresi, M., Iaccarino, S., Salvatorini, G., Turco, E., Cosentino, C., Sierro, F.J., Caruso, A., 2019. Mediterranean Neogene planktonic foraminifer biozonation and biochronology. Earth Sci. Rev. 196, 102869.
Lisiecki, L.E., Raymo, M.E., 2005. A Pliocene-Pleistocene stack of 57 globally distributed benthic δ18O records. Paleoceanography 20 (1), 1–17.
Lourens, L.J., Hilgen, F., Shackleton, N., Laskar, J., Wilson, J., 2004. The neogene period. In: Gradstein, F.M., Ogg, J.G., Smith, A.G. (Eds.), A Geologic Time Scale, 2004, pp. 409–440.
Mancilla, F.D.L., Booth-Rea, G., Stich, D., Pérez-Peña, J.V., Morales, J., Azañón, J.M., Martin, R., Giaconia, F., 2015. Slab rupture and delamination under the Betics and Rif constrained from receiver functions. Tectonophysics 663, 225–237.
Manzi, V., Gennari, R., Hilgen, F., Krijgsman, W., Lugli, S., Roveri, M., Sierro, F.J., 2013. Age refinement of the Messinian salinity crisis onset in the Mediterranean. Terra Nova 25 (4), 315–322.
Martín, J.M., Braga, J.C., Betzler, C., 2001. The Messinian Guadalhorce corridor: the last northern, Atlantic–Mediterranean gateway. Terra Nova 13 (6), 418–424.
Martín, J.M., Puga-Bernabéu, A., Aguirre, J., Braga, J.C., 2014. Miocene Atlantic-Mediterranean seaways in the Betic Cordillera (Southern Spain). Rev. Soc. Geol. Esp. 27 (1), 175–186.
Pérez-Asensio, J.N., Aguirre, J., Schmiedl, G., Civis, J., 2012a. Messinian paleoenvironmental evolution in the lower Guadalquivir Basin (SW Spain) based on benthic foraminifera. Palaeogeogr. Palaeoclimatol. Palaeoecol. 326, 135–151.
Pérez-Asensio, J.N., Aguirre, J., Schmiedl, G., Civis, J., 2012b. Impact of restriction of the Atlantic-Mediterranean gateway on the Mediterranean Outflow Water and eastern Atlantic circulation during the Messinian. Paleoceanography 27 (3).
Pérez-Asensio, J.N., Aguirre, J., Jiménez-Moreno, G., Schmiedl, G., Civis, J., 2013. Glacioeustatic control on the origin and cessation of the Messinian salinity crisis. Glob. Planet. Chang. 111, 1–8.
Pérez-Asensio, J.N., Aguirre, J., Schmiedl, G., Civis, J., 2014. Messinian productivity changes in the northeastern Atlantic and their relationship to the closure of the Atlantic–Mediterranean gateway: implications for Neogene palaeoclimate and palaeoceanography. J. Geol. Soc. 171 (3), 389–400.
Pineda, V., Artiaga, D., Ruiz-Sánchez, F.J., Montoya, P., Soria, J.M., Corbí, H., Gibert, L., 2023. New constraints on the closure of the Betic Seaway and the western Mediterranean palaeoclimate during the Messinian Salinity Crisis from the Campo Coy Basin (SE Spain). Palaeogeogr. Palaeoclimatol. Palaeoecol. 111424.
Popov, S.V., Rögl, F., Rozanov, A.Y., Steininger, F.F., Shcherba, I.G., Kovac, M., 2004. Lithological-paleogeographic maps of Paratethys-10 maps late Eocene to pliocene.
Potter, R.A., Lozier, M.S., 2004. On the warming and salinification of the Mediterranean outflow waters in the North Atlantic. Geophys. Res. Lett. 31 (1).
Raddatz, J., Rüggeberg, A., Margreth, S., Dullo, W.-C., Expedition, I., 2011. Paleoenvironmental reconstruction of Challenger Mound initiation in the Porcupine Seabight, NE Atlantic. Mar. Geol. 282 (1–2), 79–90.
Raffi, I., Wade, B., Pälike, H., Beu, A., Cooper, R., Crundwell, M., Krijgsman, W., Moore, T., Raine, I., Sardella, R., 2020. The Neogene Period, Geologic Time Scale 2020. Elsevier, pp. 1141–1215.
Ragland, P.C., 1989. Basic Analytical Petrology.
Rodrigo-Gámiz, M., Martínez-Ruiz, F., Rodríguez-Tovar, F.J., Jiménez-Espejo, F.J., Pardo-Igúzquiza, E., 2014. Millennial-to centennial-scale climate periodicities and forcing mechanisms in the westernmost Mediterranean for the past 20,000 yr. Quat. Res. 81 (1), 78–93.
Rohling, E.J., Cooke, S., 1999. Stable oxygen and carbon isotopes in foraminiferal carbonate shells. In: Modern Foraminifera. Springer, pp. 239–258.

Roveri, M., Flecker, R., Krijgsman, W., Lofi, J., Lugli, S., Manzi, V., Sierro, F.J., Bertini, A., Camerlenghi, A., De Lange, G., 2014. The Messinian salinity crisis: past and future of a great challenge for marine sciences. Mar. Geol. 352, 25–58.

Salvany, J.M., Larrasoaña, J.C., Mediavilla, C., Rebollo, A., 2011. Chronology and tectono-sedimentary evolution of the Upper Pliocene to Quaternary deposits of the lower Guadalquivir foreland basin, SW Spain. Sediment. Geol. 241 (1–4), 22–39.

Santarelli, A., Brinkhuis, H., Hilgen, F., Lourens, L., Versteegh, G., Visscher, H., 1998. Orbital signatures in a Late Miocene dinoflagellate record from Crete (Greece). Mar. Micropaleontol. 33 (3–4), 273–297.

Sanz de Galdeano, C., Alfaro, P., 2004. Tectonic significance of the present relief of the Betic Cordillera. Geomorphology 63 (3–4), 175–190.

Sanz De Galdeano, C., Vera, J.A., 1992. Stratigraphic record and palaeogeographical context of the Neogene basins in the Betic Cordillera, Spain. Basin Res. 4 (1), 21–36.

Seidenkrantz, M.-S., Kouwenhoven, T., Jorissen, F., Shackleton, N., Van der Zwaan, G., 2000. Benthic foraminifera as indicators of changing Mediterranean–Atlantic water exchange in the late Miocene. Mar. Geol. 163 (1–4), 387–407.

Selli, R., 1973. An outline of the Italian Messinian. In: Messinian Events in the Mediterranean, 7, pp. 150–171.

Sierro, F.J., 1985. The replacement of the "Globorotalia menardii" group by theGloborotalia miotumida group: An aid to recognizing the Tortonian-Messinian boundary in the Mediterranean and adjacent Atlantic. Mar. Micropaleontol. 9 (6), 525–535.

Sierro, F.J., Flores, J.A., Civis, J., González Delgado, J.A., Francés, G., 1993. Late Miocene globorotaliid event-stratigraphy and biogeography in the NE-Atlantic and Mediterranean. Mar. Micropaleontol. 21 (1–3), 143–167.

Sierro, F.J., González-Delgado, A., Dabrio, C.J., Flores, A., Civis, J., 1996. Late Neogene depositional sequences in the foreland basin of Guadalquivir (SW Spain). In: Friend, P.F., Dabrio, C.J. (Eds.), Tertiary Basins of Spain. Cambridge University Press, Cambridge, pp. 339–345.

Sierro, F.J., Hilgen, F.J., Krijgsman, W., Flores, J.A., 2001. The Abad composite (SE Spain): a Messinian reference section for the Mediterranean and the APTS, 168 (1–2), 141–169.

Sierro, F.J., Hodell, D.A., Andersen, N., Azibeiro, L.A., Jimenez-Espejo, F.J., Bahr, A., Flores, J.A., Ausin, B., Rogerson, M., Lozano-Luz, R., 2020. Mediterranean overflow over the last 250 kyr: freshwater forcing from the tropics to the ice sheets. Paleoceanogr. Paleoclimatol. 35 (9) e2020PA003931.

Tjalsma, R.C., 1971. Stratigraphy and foraminifera of the Neogene of the eastern Guadalquivir Basin (southern Spain). Utrecht University.

Tulbure, M., Capella, W., Barhoun, N., Flores, J., Hilgen, F., Krijgsman, W., Kouwenhoven, T., Sierro, F.J., Yousfi, M.Z., 2017. Age refinement and basin evolution of the North Rifian Corridor (Morocco): No evidence for a marine connection during the Messinian Salinity Crisis. Palaeogeogr. Palaeoclimatol. Palaeoecol. 485, 416–432.

Van den Berg, B.C.J., Sierro, F.J., Hilgen, F.J., Flecker, R., Larrasoaña, J.C., Krijgsman, W., Flores, J.A., Mata, M.P., Bellido Martín, E., Civis, J., González-Delgado, J.A., 2015. Astronomical tuning for the upper Messinian Spanish Atlantic margin: Disentangling basin evolution, climate cyclicity and MOW, 135, 89–103.

Van den Berg, B.C.J., Sierro, F.J., Hilgen, F.J., Flecker, R., Larrasoaña, J.C., Krijgsman, W., Flores, J.A., Mata, M.P., 2018. Imprint of Messinian Salinity Crisis events on the Spanish Atlantic margin. Newsl. Stratigr. 51 (1), 93–115.

Van der Schee, M., Van den Berg, B.C., Capella, W., Simon, D., Sierro, F.J., Krijgsman, W., 2018. New age constraints on the western Betic intramontane basins: A late Tortonian closure of the Guadalhorce Corridor? Terra Nova 30 (5), 325–332.

Voelker, A.H., Lebreiro, S., Schönfeld, J., Cacho, I., Erlenkeuser, H., Abrantes, F., 2006. Mediterranean outflow strengthening during northern hemisphere coolings: a salt source for the glacial Atlantic? Earth Planet. Sci. Lett. 245 (1–2), 39–55.

Westerhold, T., Marwan, N., Drury, A.J., Liebrand, D., Agnini, C., Anagnostou, E., Barnet, J.S., Bohaty, S.M., De Vleeschouwer, D., Florindo, F., 2020. An astronomically dated record of Earth's climate and its predictability over the last 66 million years. Science 369 (6509), 1383–1387.